Published in final edited form as:
Acta Biomater. 2012 October ; 8(10): 3561–3575. doi:10.1016/j.actbio.2012.06.034.

In vivo effects of L1 coating on inflammation and neuronal health at the electrode/tissue interface in rat spinal cord and dorsal root ganglion

Christi L. Kolarcik[a], **Dennis Bourbeau**[b], **Erdrin Azemi**[a,c], **Erika Rost**[a], **Ling Zhang**[a], **Carl F. Lagenaur**[c,d], **Douglas J. Weber**[b], and **X. Tracy Cui**[a,c,e]

[a]Department of Bioengineering, University of Pittsburgh, Pittsburgh, PA USA

[b]Department of Physical Medicine and Rehabilitation, University of Pittsburgh, Pittsburgh, PA USA

[c]Center for the Neural Basis of Cognition, University of Pittsburgh, Pittsburgh, PA USA

[d]Department of Neurobiology, University of Pittsburgh, Pittsburgh, PA USA

[e]McGowan Institute for Regenerative Medicine, University of Pittsburgh, Pittsburgh, PA USA

Abstract

The spinal cord (SC) and dorsal root ganglion (DRG) are target implantation regions for neural prosthetics, but the tissue-electrode interface in these regions is not well-studied. To improve our understanding of these locations, we characterized the tissue reactions around implanted electrodes. L1, an adhesion molecule shown to maintain neuronal density and reduce gliosis in brain tissue, was then evaluated in SC and DRG implants. Following L1 immobilization onto neural electrodes, the bioactivities of the coatings were verified *in vitro* using neuron, astrocyte and microglia cultures. Non-modified and L1-coated electrodes were implanted into adult rats for 1 or 4 weeks. Hematoxylin and eosin staining along with cell-type specific antibodies were used to characterize the tissue response. In the SC and DRG, cells aggregated at the electrode-tissue interface. Microglia staining was more intense around the implant site and decreased with distance from the interface. Neurofilament staining in both locations was decreased or absent around the implant when compared to surrounding tissue. With L1, neurofilament staining was significantly increased while neuronal cell death decreased. Our results indicate that L1-modified electrodes may result in an improved chronic neural interface and will be evaluated in recording and stimulation studies.

Keywords

electrode; interface; biocompatibility; neural prosthesis; surface modification

Corresponding author: X. Tracy Cui, Ph.D., Department of Bioengineering, University of Pittsburgh, 5057 Biomedical Science Tower 3, 3501 Fifth Avenue, Pittsburgh, PA 15260, Ph: +1-412-383-6672, Fax: +1-412-383-5918, xic11@pitt.edu.

Disclosures

The authors have no potential conflicts of interest.

1.1 Introduction

Neural prosthetic devices implanted into the nervous system to bypass and/or restore sensory-motor or cognitive functions have enormous clinical potential. There are a variety of situations in which such devices can be of use with proposed applications in the fields of gerontology, rehabilitative medicine, psychiatry, neurology and clinical research [1]. More specifically, neural interface systems (NIS) can be used for communication [2], to restore lost functional movement [3], to reinnervate target locations for bladder control and for the treatment of neurological conditions like epilepsy [4, 5] and Parkinson's Disease [6] among others. While much effort has been devoted to brain interfaces, both the spinal cord (SC) and dorsal root ganglion (DRG) are target implantation regions for these promising rehabilitative and therapeutic devices as well. For example, SC stimulation has been investigated for pain control [7] and restoration of motor functions [8, 9], while the DRG is an attractive site for recording or stimulating primary afferent neurons to provide sensory feedback [10, 11].

Irrespective of the implant location, these neural interfaces must remain stable throughout the lifespan of the user. However, biocompatibility issues have limited the success of chronically implanted devices [12–15]. The fate of implanted devices is often determined by the effective integration with the surrounding neural tissue, a current and major roadblock in neuroengineering [1, 16–18]. In brain tissue, immune and inflammatory reactions including gliosis at the implant site result in decreased performance of microelectrodes. Gliosis is thought to be mediated by macrophages, activated microglia and reactive astrocytes resulting in the formation of a glial sheath that can encapsulate and isolate the implanted probe from the surrounding tissue [19]. In addition, significant decreases in neuronal density in the area immediately surrounding the implant site (the "kill zone") are problematic. For the long-term success of chronically-implanted electrodes, maintaining neurons close to the implant site (within 50–100 μm), minimizing astrogliosis and reducing or eliminating microglial activation are necessary. In the peripheral system, manipulation or damage to a neural structure also leads to anatomic, metabolic and physiological alterations [20]. However, the reactions surrounding these peripheral interfaces highlight the potential for nerve regeneration and recovery following initial damage [20–22]. Although valuable for multiple applications, the SC and DRG are less well-studied than the brain and peripheral nerve. Therefore, our first aim in this study is to fully characterize the tissue responses in the SC and DRG at both acute and chronic time points in an effort to better understand the cellular responses specific to each.

Surface modifications of implanted electrodes are one approach used to promote favorable interactions between the neural implants and neural cells, and a variety of biomaterial designs have been investigated [2, 16]. Previous work by our laboratory indicates that the immobilization of L1, a neural adhesion molecule, onto the surface of probes implanted in the rat cortex specifically promotes neuronal survival and neurite outgrowth while inhibiting glial cell proliferation [23]. L1, a transmembrane cell surface glycoprotein, mediates cell-cell recognition by interacting with L1 molecules on the surfaces of neighboring cells ("hemophilic interactions") or with non-L1 molecules on the surfaces of these cells ("heterophilic interactions") [24, 25]. It is one of the molecular cues that promotes neurite outgrowth [26, 27] thereby contributing to the formation of the complex neuronal connections of the nervous system [25]. It is also involved in neuronal migration and synaptic plasticity with essential roles in the maintenance of nervous system functions [24, 28]. L1 serves as a survival factor for neurons of the central nervous system (CNS) [29–31] and is involved during regenerative responses in the adult CNS [32]. In fact, transplantation of cells engineered to express L1 was associated with improved recovery following spinal cord injury [33–35]. Furthermore, L1 mediates peripheral myelin formation [36]. This evidence indicates that coating electrodes with L1 may improve their biocompatibility when

implanted into either the SC or DRG. Therefore, the second goal of the current study was to investigate the ability of L1 to improve the implant-tissue interface. Our previous *in vitro* [19] and *in vivo* [23] work indicates that L1 is able to reduce inflammatory gliosis while promoting/maintaining neuronal health. We hypothesized that electrodes coated with L1 and implanted into the SC or DRG will exhibit a reduced inflammatory response and an increase in neuronal density when compared to non-modified (NM) control probes at both acute and chronic time points. Immunohistological evaluation of the tissue response associated with each probe was quantified and compared by implant site (SC versus DRG), time point (1 week versus 4 weeks) and coating (L1 versus NM).

2.1 Materials and Methods

2.1.1 Neural Probes and Surface Modification

Standard tip tungsten microelectrodes (MicroProbes, Gaithersburg, MD) were used for both *in vitro* experiments and *in vivo* implants. Each microelectrode was cut to a 3 mm length for chronic insertion into the neural tissue. The shaft diameter of these tips was approximately 0.081 mm (with a parylene-C coating of 3 μm) and an exposed tip diameter of 1–2 μm (25:1 taper).

L1 protein was purified as described previously [19, 27] and concentrations determined using the FluoroProfile (Sigma-Aldrich, St. Louis, MO) epicocconone-based reagent kit [37] using bovine serum albumin (BSA; Sigma-Aldrich) standards. All coating experiments were carried out in a sterile environment at room temperature. A two-step approach similar to that used by Musalla and colleagues was utilized [38]. More specifically, parylene-C-insulated microwires were treated with plasma for 10 seconds. Then two different protein solutions, L1 (100 μg/mL) or laminin (40 μg/mL, Sigma–Aldrich), were added onto the parylene-C/plasma-modified surfaces for 1 hour at 4°C. The coating conditions included the following: 1.) untreated parylene-C, 2.) parylene-C + plasma treatment, 3.) parylene-C + plasma treatment + L1 and 4.) parylene-C + plasma treatment + laminin.

Neural probes for the *in vivo* studies were sterilized with ethylene oxide (EtO). The L1 group was treated with plasma for 10 seconds on each side and L1 deposited as described above for 1 hour at 4°C. The resulting L1-immobilized probes were rinsed with phosphate buffered saline (PBS, pH 7.4) and stored at 4°C in sterile PBS until implantation. The L1 coating was performed the same day of the implantation.

2.1.2 Cell Culture

L1 immobilization was confirmed by staining with the 5H7 L1 monoclonal primary antibody and fluorophore-conjugated secondary antibody as described [19]. The stability of the coatings was tested at two time points. For the day 0 time point, cells were plated on the same day as the coating was applied. For the day 5 time point, cells were added to the coated surface 5 days after the coating had been soaked in Dulbecco's Modified Eagle Medium (DMEM) without serum at 37°C and 5% CO_2. For visualization of the protein coating, fluorophone-conjugated antibody was immobilized on the microwires and coating localization visualized using bright-field and fluorescence microscopy.

Rat cortices from embryonic day 18 (E18) Sprague-Dawley rats were obtained from BrainBits, LLC (Springfield, IL) and neuronal cultures prepared as described by Brewer and colleagues [39]. Cells were resuspended in neurobasal base media (Invitrogen, Carlsbad, CA) supplemented with B27 (Invitrogen), glutamine (Sigma-Aldrich) and glutamate (Sigma-Aldrich). Cells were plated on surface-modified parylene-C at a density of 1.5×10^5 cells/cm^2 and maintained in culture for 3 days at 37°C and 5% CO_2.

Astrocyte-enriched cultures were prepared as described previously [19]. Briefly, rat cortices were digested with trypsin and the resulting cell suspension maintained in DMEM (Invitrogen) supplemented with 10% fetal calf serum (FCS; Thermo Scientific, Pittsburgh, PA) at 37°C and 5% CO_2. Glial cells were passaged weekly for up to 4 weeks. For surface modification experiments, glial cells were trypsinized, resuspended in DMEM/10% FCS and plated at a density of 1.5×10^5 cells/cm^2. Astrocytes were subsequently cultured for 2 days prior to fixation.

Highly Aggressively Proliferating Immortalized (HAPI) cells [40] were used to investigate the microglial response to the various surface modifications *in vitro* and were kindly provided by Dr. Xiaoming Hu, Department of Neurology, University of Pittsburgh. These cells were cultured as described previously [41]. Briefly, HAPI cells were maintained in DMEM/F12 lacking HEPES and Phenol Red (Invitrogen) supplemented with L-glutamine (Sigma-Aldrich) and 10% fetal bovine serum (FBS; Thermo Scientific). After thawing, cells were passaged once prior to plating at a density of 1×10^5 cells/cm^2 and incubated for 24 hours at 37°C and 5% CO_2 before fixation.

Prior to immunohistochemical labeling, cells were fixed with 4% paraformaldehyde (PFA; Sigma-Aldrich) for 10 minutes. After blocking for 45 minutes with 4% goat serum in phosphate buffered saline (PBS), monoclonal antibodies for neuronal class III β-tubulin (2 μg/mL; Invitrogen), glial fibrillary acidic protein (0.4 μg/mL; GFAP; DakoCytomation, Carpinteria, CA) and ED1 (4 μg/mL; Fisher Scientific, Pittsburgh, PA) were added for 1 hour at room temperature. After washing with PBS, fluorescence-conjugated secondary antibodies were added for 1 hour. Cell nuclei were stained with Hoechst 33258 (2 μg/mL; Sigma-Aldrich) in PBS. Ten samples for each coating condition were used for each experiment and experiments were repeated at least three times.

Digital images of the stained cells were taken using a fluorescence microscope (Zeiss Axioskop, Zeiss, USA). Neuronal attachment was determined by counting the number of neurons that showed co-localization of class III β-tubulin and Hoescht and had at least one neurite longer than the cell body dimensions. Astrocyte attachment was determined for cells that showed co-localization of GFAP and Hoescht. Microglia attachment was determined by the co-localization of ED1 and Hoescht. The entire probe was imaged and all cells on the surface of the probes were counted by an unbiased examiner. The cell number was reported by dividing the total number of cells by the projected surface area. Statistical analyses were performed using GraphPad Prism 5 (GraphPad Software, Inc., La Jolla, CA). Comparisons involving multiple groups were accomplished using two-way analysis of variance (ANOVA) followed by Bonferroni post-hoc analysis. A p value ≤ 0.05 was considered statistically significant.

2.1.3 Surgical Procedure

All surgical procedures were done in accordance with those outlined by the United States Department of Agriculture and approved by the Institutional Animal Care and Use Committee of the University of Pittsburgh. Animals were housed in the facilities of the University of Pittsburgh Department of Laboratory Animal Resources and given free access to food and water.

Twenty-four adult male Sprague-Dawley rats (300 ± 50 g) were used throughout this study. Three or four animals per time point were implanted in the spinal cord (SC) and/or dorsal root ganglion (DRG) with either non-modified or L1-coated microelectrode tips (outlined in Table 1). Both 1 week and 4 week time points were investigated in an effort to characterize the acute (1 week) and chronic (4 weeks) tissue responses.

Animals were anesthetized with 2.5% isofluorane in oxygen at 1 L/min for 5 minutes prior to surgery and then maintained for the duration of the procedure with 1–2% isofluorane. Anesthesia level was closely monitored during the procedure by observing changes in respiratory rate, heart rate, body temperature and absence of the pedal reflex. Ophthalmic ointment was applied to the eyes while animals were under anesthesia.

Animals were placed in a stereotaxic frame and the hair over the incision site removed. The skin was disinfected with isopropyl alcohol and betadine and a sterile environment maintained throughout the procedure. The lumbar spine was exposed through a dorsal midline incision using surgical elevators to clear soft tissue from bone. A unilateral laminectomy exposed the left side of the lumbar spinal cord and DRG. Every attempt was made to minimize removal and/or cutting of muscles and bone surrounding the area of implant. Once exposed, non-modified or L1-coated probes (~3 mm length) were inserted (1–4/SC and 1–2/DRG) under a surgical microscope using a micromanipulator equipped with a vacuum tool; probes were held in place with the vacuum tool, positioned by moving the micromanipulator and then lowered into place. After the muscle and skin were sutured, the animal recovered under close supervision in the surgical procedure room. Rats were monitored closely for signs of pain or distress and post-operative pain managed with buprenorphine (0.3 mg/kg). The same surgeon performed all surgeries to minimize variability associated with the surgery and electrode implantation.

2.1.4 Tissue Preparation and Immunofluorescence

At the designated time points, animals were anesthetized with a ketamine/xylazine cocktail (100/20 mg/kg) via the intraperitoneal (IP) cavity. Animals were then transcardially perfused with cold (4°C) PBS followed by 4% (w/v) PFA in PBS. The spinal cord/DRG tissue was removed, post-fixed for up to 3 days and then equilibrated in 30% sucrose. Dissected tissue was then cryoprotected using the optimal cutting temperature (OCT) compound (Tissue-Tek, Torrance, CA). Serial sections were cut at a 10 μm thickness.

Monoclonal antibodies were used to detect neurofilament 200 kD (NF200; Millipore, Billerica, MA), vimentin (Clone V-9; Millipore) and neuronal nuclei (NeuN; Millipore). Polyclonal antibodies were used to detect Iba1 (Wako Chemicals USA, Inc., Richmond, VA), glial fibrillary acidic protein (GFAP; DakoCytomation) and cleaved caspase-3 (Asp175; Cell Signaling Technology, Boston, MA). These antibodies were used at a dilution of 1:500 (NF200, Iba1, Vimentin, GFAP, NeuN) or 1:50 (cleaved caspase-3) and the appropriate fluorescence-conjugated antibody used at a dilution of 1:500.

Tissue sections were stained at the same time for each antibody/antibody pair to minimize variability. Hematoxylin and eosin (H and E) staining along with markers to visualize mature axons (NF200), microglia (Iba1), astrocytes/fibroblasts/endothelial cells (vimentin), astrocytes (GFAP), neuronal nuclei (NeuN) and cell death (cleaved caspase-3) (antibodies outlined in Table 2) were used.

Tissue sections were hydrated in PBS and non-specific binding blocked with 0.5% BSA. Primary antibodies were then diluted in BSA and added for approximately 1 hour. After washing with BSA, fluorophore-conjugated secondary antibodies (goat anti-mouse Alexa Fluor 488 and goat anti-rabbit Alexa Fluor 594) diluted in BSA were added for approximately 1 hour and Hoescht used as the nuclear stain. Fluoromount-G (Southern Biotechnology Associates, Birmingham, AL) was used for mounting and to preserve fluorescence. Negative controls lacking primary antibody were included for each secondary antibody.

2.1.5 Quantitative tissue and statistical analyses

Confocal fluorescent microscopy was used to evaluate the cellular reactions associated with the implanted electrodes. Images were acquired using an Olympus Fluoview 1000 I Confocal Microscope (Olympus America, Center Valley, PA) at the Center for Biologic Imaging at the University of Pittsburgh. For each antibody, images were acquired using the same exposure time and in a single session to reduce variability during data analysis. Images were centered on the implant site and multiple images acquired. Images were also taken in sections of tissue lacking an implant (although from the same slide) and used to define the average background staining intensities for each stain on every tissue sample.

For quantification of NF200 staining, custom MATLAB software (MathWorks, Boston, MA) was used to determine the size of the kill zone. More specifically, the perimeter of each implant site was defined using the corresponding DAPI-stained image and the NF200-stained image used to identify the presence of NF200 staining (indicative of intact neuronal processes). The size of the kill zone was then calculated in 10° bins around the 360° perimeter of the implant site by subtracting the location of the implant site from the location of NF200 staining. These 36 distance measures were used to calculate the mean kill zone size and compared via the rank sum test. Box and whisker plots were used to highlight the 5^{th}, 25^{th}, 50^{th}, 75^{th} and 95^{th} percentiles for each coating at each time point in each location.

For quantification of Iba1 and GFAP staining, DAPI-stained images were again used to determine the perimeter of the implant site. Threshold values based on 95% of the background staining for each section were established. The amount of staining above this threshold value was then quantified and reported as a function of distance from the implant site. The median intensity values were binned every 50 μm from the implant site and compared via the rank sum test.

For NeuN/caspase-3 stained images, the number of NeuN/caspase-3 positive cells was quantified and reported as a percentage of the total number of NeuN positive cells.

Comparisons between any two groups of data were accomplished using the unpaired t test at the 95% confidence interval. A p value ≤ 0.05 was considered statistically significant.

3.1 Results

3.1.1 In Vitro Studies

To determine if the L1 coating could increase neuronal density and decrease gliosis, we quantified and compared the cellular attachment of neurons, astrocytes and microglia for the different surface conditions (Figure 1). We chose to use parylene-C insulated probes as the implant model because a number of widely used neural electrode arrays include parylene-C as the insulator. We utilized a two-step approach to immobilize proteins onto the parylene-C surface. Plasma treatment was first used to provide a charged polar group at the surface to facilitate protein binding. Protein was then adsorbed onto the activated surface. The effectiveness of protein immobilization was verified by testing the cellular response in culture. In comparison to the uncoated probes, a higher number of neurons were observed on the L1- and laminin-coated probes while there were fewer activated microglia. However, there were significantly fewer astrocytes on the L1-coated probes than on the laminin-coated probes (Figure 1). This difference is consistent with the known bioactivities of the two proteins. That is, L1 is a neuron-specific adhesion molecule that promotes growth and adhesion via hemophilic binding while laminin is an extracellular matrix protein that binds to multiple cells types via the integrin receptors. Therefore, the coating method was effective in immobilizing proteins and maintaining their respective biological functionality. In addition, the cellular responses associated with wires coated with proteins and soaked in

media for 5 days were similar to those observed with freshly-coated wires (Figure 1B) indicating that these proteins remain stable on the plasma-treated surfaces. Using fluorescence microscopy, the attachment of proteins was found to be predominantly on the shaft, not on the tip of the probe and the distribution is uniform along the shaft (Figure 1C and 1D). As the L1-coated microwires demonstrated the desired properties for an improved neural tissue interface *in vitro* (i.e., increased neuronal attachment and decreased adhesion/activation of glial cells), we utilized this surface modification for subsequent *in vivo* work and evaluated the tissue response along the electrode shaft.

3.1.2 Characterization of the tissue response in the SC

We performed a number of histological stains to evaluate and characterize the tissue reaction in response to the NM and L1-coated electrodes (antibodies outlined in Table 2). First, to determine the degree of neuronal and axonal loss around the implant site, NF200 was used. In the SC, NF200 staining is decreased or absent in the area immediately surrounding the implant site (Figure 2). This area, termed the kill zone, was evident at both 1 week (Figure 2A) and 4 week (Figure 2B) time points. MATLAB was used to quantify kill zone sizes which were then compared via the rank sum test. In the SC and at both time points, the size of the kill zone was significantly reduced ($p < 0.001$) with the L1 coating as compared to the NM microelectrodes (Figure 3).

We also sought to characterize the non-neuronal cell response including the reactions associated with microglia/macrophages, astrocytes and fibroblasts using Iba1, GFAP and vimentin antibodies, respectively. Cells that stained positive for Iba1 were localized to the area immediately surrounding the implant. The staining intensity was greatest at the interface and decreased in intensity further from the implant (Figure 2). MATLAB was again utilized to assess the decay in Iba1 staining. For this analysis, decay as a function of distance from the implant site was graphically represented and the median intensity values in 50 μm bins were compared via the rank sum test (as shown in Figure 4). In the SC, there was little difference between NM and L1-coated electrodes at the 1 week time point (Figure 4A). However, at 4 weeks, the intensity of Iba1 staining was significantly higher with the NM electrodes (Figure 4B).

GFAP-positive cells, identified as reactive astrocytes, resulted in the formation of a sheath a short distance from the electrode-tissue interface (Figure 5). Vimentin-positive cells were localized at and around the implant site with some co-localization with GFAP (Figure 5). Cells that were vimentin positive and GFAP negative were identified as microglia, endothelial cells and fibroblasts. To quantify GFAP staining, the same MATLAB analyses used for Iba1 staining quantification were used. In the SC, there was little difference in GFAP staining intensity between acute and chronic time points (Figure 6) although there were significant differences between the NM and L1 electrodes between 50–150 μm at 1 week and 150–300 μm at 4 weeks (Figure 6).

Finally, to determine the impact on neuronal cell death, the colocalization of NeuN and activated caspase-3 was determined (example images provided in Figure 7). In the SC, L1-coated electrodes were associated with a decrease in the percentage of neuronal cell death as assessed by the number of NeuN/caspase-3 positive cells versus NeuN positive cells at both acute and chronic time points (Table 3).

3.1.3 Characterization of the tissue response in the DRG

The same histological stains used in the SC were also used to assess the tissue response in the DRG. For NF200, staining intensity was decreased or absent in the area immediately surrounding the implant site (Figure 8). Again, this kill zone was evident at both acute

(Figure 8A) and chronic (Figure 8B) time points. In the DRG as in the SC, the size of the kill zone was significantly reduced at both time points with the L1 coating as compared to the NM microelectrodes ($p < 0.001$; Figure 9).

For Iba1 staining, we observed a significant decrease in staining intensity at the 1 week time point in the DRG with the L1 coating (Figures 8A and 10A). Interestingly, the intensity of Iba1 staining was higher in the L1-modified group in the DRG at the 4 week time point when compared with the NM probes (Figures 8B and 10B).

In the DRG, there was a significant decrease in GFAP staining intensity at the 1 week time point with the L1 coating (Figures 11 and 12A). However, the intensity of GFAP staining was increased in the DRG at the 4 week time point at distances up to 150 μm from the interface with L1-coated microelectrodes (Figure 11 and 12B).

Finally, L1-coated electrodes in the DRG were associated with a decrease in the percentage of neuronal cell death at both time points analyzed (Figure 13 and Table 3) as observed in the SC.

4.1 Discussion

One of the remaining challenges in the development of long-term neural interfaces or neuroprosthetics is maintenance of the cellular environment surrounding the implant. In particular, preventing neuronal cell death, promoting neuronal health and minimizing the inflammatory response are critical for success. Both central and peripheral nervous system sites including the SC and DRG, respectively, are important target implant sites for such devices. In this study, we have compared the cellular response in these less well-studied locations at both acute and chronic time points and then investigated the ability of L1 surface modifications to improve the tissue-electrode interface. Our results indicate that neuronal density and health are significantly improved in the presence of the L1 surface modification in both central and peripheral locations.

4.1.1 The cellular response to implanted electrodes in the SC and DRG

As potential sites for interfacing with neural prosthetics, it is important to understand the tissue response to neural probes implanted in the SC and DRG. In the SC, we observed a significant decrease in the amount of staining for neuronal processes immediately surrounding implant sites for non-modified probes (Figure 2, top panels in A and B). This kill zone was apparent at both the acute and chronic time points. However, the size of the kill zone was significantly larger at the 1 week time point (median size of 174.56 μm) than at the 4 week time point (median size of 145.56 μm; $p < 0.001$) suggesting some degree of axonal regeneration following injury. The extent and nature of this regeneration in the absence of coating could be better characterized in future studies using additional time points.

In the central nervous system, microglia are resident cells that are activated along with astrocytes in response to injury. In both central and peripheral tissues, invading cells express Iba1, a calcium binding protein localized exclusively to microglial cells in the nervous system [42, 43]. This protein plays an important role in cell migration and mediates the phagocytic activity of microglia [44]. Iba1 is also up-regulated in a variety of conditions indicating its importance in the activated microglial phenotype [42, 44–46]. For the Iba1-mediated component of the inflammatory response, we observed increased staining in the area immediately surrounding the implant with levels reaching that of the background as the distance from the interface increased. Although both acute and chronic time points experienced this decay as a function of distance, the overall intensity of the Iba1 response

was significantly greater at the 1 week time point at distances ranging from 0–250 μm (0–50 μm, $p < 0.01$; 50–100 μm, $p < 0.01$; 100–150 μm, $p < 0.05$; 150–200 μm, $p < 0.001$; 200–250 μm, $p < 0.05$). Astrocyte staining patterns for the uncoated probes were characterized by a sheath a short distance from the interface. Again, the formation of this glial scar was observed at both time points with a decline in staining intensity to background levels as the distance from the interface increased. However, there was a significant increase in the intensity of GFAP staining between 50 and 100 μm at the 4 week point ($p < 0.01$) suggesting that the uncoated probes continued to promote astrocyte migration after the acute injury. Vimentin staining was also assessed as this protein is expressed by a number of cell types including immature and reactive astrocytes, microglia, endothelial cells and fibroblasts. In this study, vimentin appeared to be confined closer to the implant interface than GFAP indicating the presence of fibroblasts closer to the implant site due to initial vascular injury.

Apoptosis, a process that occurs throughout development, also occurs following damage to the nervous system by a variety of conditions including traumatic spinal cord injuries [47, 48]. It is a well-established secondary injury mechanism and is distinct from necrosis, a form of cell death characterized by membrane lysis, release of intracellular contents and inflammation [49, 50]. When activated, apoptotic cascades occur in neurons, oligodendrocytes, microglia and possibly astrocytes [51, 52] Although a major apoptotic trigger is calcium influx, other insults including cytokines, inflammatory injury, excitotoxicity and free radical damage can impact cells farther from the injury site [47, 53, 54]. As caspase-3 mediated apoptotic cell death was observed in the SC, preventing or minimizing this secondary mechanism of damage will be critical for the long-term performance of any neuroprosthetic. Additional markers can be utilized in future studies to visualize degenerating axons and to better characterize caspase-independent forms of cell death.

The response observed in the DRG was similar in many ways to that observed in the SC. For example, a decrease in the amount of neuronal process staining in the kill zone was observed in this peripheral site and at both time points studied (Figure 8, top panels in A and B). The size of the kill zone was significantly larger at the 1 week time point (median size of 190.18 μm) than at the 4 week time point (median size of 148.65 μm; $p < 0.001$) again suggesting a regenerative process following injury.

In peripheral tissues like the DRG, it is believed that immune cells also invade following injury [55, 56] and some of these cells express Iba1. We found that the Iba1-mediated component of the inflammatory response in the DRG resembled that of the SC. Iba1 staining in the area immediately surrounding the implant was increased and levels reached that of the background with increasing distance from the interface. In comparing the 1 and 4 week time points, the overall intensity of the Iba1 response was significantly greater at the 1 week time point at distances up to 350 μm from the interface (0–50 μm, $p < 0.001$; 50–100 μm, $p < 0.001$; 100–150 μm, $p < 0.001$; 150–200 μm, $p < 0.001$; 200–250 μm, $p < 0.01$; 250–300 μm, $p < 0.05$; 300–350 μm, $p < 0.05$). The GFAP staining observed in the DRG can be attributed to satellite glial cells (SGCs) which ensheath the DRG perikarya after injury [57] and are thought to control the neuronal microenvironment in the DRG [58]. Further studies are required to elucidate the exact role of these cells in our model and to better characterize their response in the presence of L1.

Finally, caspase-3-mediated neuronal apoptosis was also observed in the DRG as in the SC. The extent of this form of cell death in neurons as well as in supporting cells can be further characterized in future studies. However, it should be noted that neuronal cell death does not fully explain the observed loss of NF200 staining in either the SC or DRG; dendritic

retraction and microglial recruitment/neuronal cell exclusion are both likely to contribute to kill zone size as well.

In comparing our previous work in the brain with the current study, more dramatic loss of cells around the implant site and differences in Iba1-related response were found in the SC and DRG. This may be a result of mechanical and motion differences between the brain and SC/DRG resulting in a smoother insertion and less relative motion in the brain. It is well-documented that the mechanical properties of current electrode materials are significantly different from those of the brain. In particular, the elastic moduli of materials like tungsten and silicon are seven to eight orders of magnitude greater than that of brain tissue. This disparity can augment both the foreign body response with “frustrated phagocytosis” [15] as well as the inflammatory response [59]. While not new to the field of tissue engineering in general [60–62], matching the mechanical properties of implanted scaffolds or devices with those of the surrounding tissue should minimize mismatch-associated damage caused by micro-motion and/or the foreign body response. Therefore, soft materials with mechanical properties similar to those of CNS or PNS tissue must be considered to prevent or limit these problems, and a number of groups are working to develop such interfaces [63–66].

4.1.2 Effects of the L1 coating

In terms of neuronal presence around the implants, we observed significant decreases in the size of the kill zone with the L1 coating at both 1 week and 4 weeks and in the SC (Figure 3) and DRG (Figure 9). In the SC, the decrease in kill zone size with the NM probes between 1 and 4 week time points was not observed although the variability in kill zone size after 1 week was decreased at the 4 week time point with L1. This suggests that L1 may prevent the dramatic loss of neuronal processes seen with NM probes and that, combined with the inherent regenerative capacity of the CNS, an improved electrode/tissue interface is achieved with the L1 coating.

In addition, neuronal health appeared to improve in the presence of L1 as a significantly lower percentage of neurons were positive for activated caspase-3, an important cellular mediator of programmed cell death (Figures 7 and 13 and Table 3). This may be due to the regenerative responses associated with L1 following nervous system injury. This correlation has been well-studied *in vitro* using a number of cell types (reviewed in [67]) and in adult zebrafish using an L1 homolog [68, 69]. Although the *in vivo* evidence is less abundant, studies in mouse models of Parkinson’s disease and in spinal cord injury models indicate that L1 can improve cell survival as compared to controls lacking L1 expression [70, 71]. Taken together, these results indicate that the L1 immobilized on the implanted microelectrodes can promote regeneration of injured neurons or axons near the implant site.

In the SC, our analyses indicate that Iba1 staining intensity only differed between NM and L1-coated microelectrodes at distances 50–100 μm from the implant site at the early time point although at the 4 week time point there was a significant decrease in Iba1 staining intensity with the L1 coating at distances 50–300 μm from the implant site. In the DRG, we observed a decrease in Iba1 staining intensity with L1 at the 1 week time point and then an increase in Iba1 intensity with L1 at the 4 week time point. It is difficult to interpret the effects of L1 on microglia/macrophages as this interaction in both central and peripheral nervous systems has yet to be fully characterized. In order to better understand the interaction between these immune cells and L1, additional longitudinal studies could be performed to characterize changes in cellular adhesion and phenotype over time. More specific staining could be incorporated in these future studies to identify different microglia/macrophage phenotypes. As microglia/macrophages can have distinct functions ranging from pro-inflammatory and degenerative to anti-inflammatory and neuroprotective [72, 73],

it is important to determine how L1 may impact these functions particularly if it can promote the latter set of responses.

Reactive astrogliosis is a prominent response of the central nervous system to injury and can be characterized by increased expression of GFAP, cell and process enlargement and proliferation [74]. This leads to local accumulation of astrocytes and formation of what is termed the glial scar, characterized by the deposition of a dense extracellular matrix [67]. Although we did not observe a significant difference in GFAP staining intensity in the SC with the L1 coating, GFAP immunoreactivity for both NM and L1-modified probes increased as a function of time as reported previously [23]. As reported by other groups, reactive astrocytes progressively displace neurons away from the recording zone, a mechanism that likely accounts for failure during single unit recordings in the brain [15, 75]. However, evidence suggests that this scar may not be an impermeable barrier as a result of axon growth- and cell migration-promoting immunoglobulin cell adhesion molecules (IgCAMs) like L1 [67]. In fact, specific types of IgCAMs can promote the ingrowth of axons into the scar. Roonprapunt and colleagues found that by infusing a soluble L1 fragment into the scar, axon regrowth across the scar was significantly enhanced [76]. Additional work using L1 to promote this type of ingrowth is certainly warranted and indicates a promising avenue for therapeutic interventions.

Finally, in the SC, L1-coated microelectrodes showed a significant decrease in vimentin activity at both time points as compared to the NM probes. This response is consistent with our previous work in the brain [23] as well as with another study showing that L1 is inhibitory to fibroblast attachment *in vitro* [77].

A variety of methods are currently being investigated to prevent cellular encapsulation and electrode failure and can generally be divided into those that involve surface modifications meant to interact with the electrode microenvironment and those that gradually release soluble factors. Surface immobilization of biomolecules is expected to work by directing host cells to interact specifically with the bioactive species anchored on the surface of the implant. Only the cells immediately surrounding the implant will be directly affected and the time frame for interaction is early on, although secondary effects may extend to a larger spatial and temporal zone via signaling cascades. L1 is an example of this type of coating and continues to show promise in promoting neuron-specific attachment. Laminin has also been evaluated [78] as well as molecules designed to prevent astrocyte attachment [79]. These coatings may promote the survival and growth of neurons and neurites, but if inflammation is severe, these effects may not be sufficient especially in the long-term. Conversely, the release of anti-inflammatory drugs [80] or neuropeptides [81] may allow soluble factors to achieve better interaction volumes and provide greater control of the delivery schedule. Although this may reduce both the acute and chronic inflammatory response, these coatings will lack an intimate connection between the implant surface and neurons which could translate to poor recording quality and signal drift. Nevertheless, each of these surface modifications is encouraging although it is likely that a combination of these and other approaches will prove most effective.

5.1 Conclusions

In the current study, we have reported on the cellular responses associated with implanting L1-coated tungsten microelectrodes into the SC and DRG. We have demonstrated that immobilization of neuron-specific L1 protein significantly promotes neuronal density and neuronal health at the tissue interface at both acute and chronic time points. These results are consistent with previous work by our laboratory and suggest that immobilization of L1 may increase the biocompatibility of neural probes used both centrally and peripherally for

rehabilitative and therapeutic purposes. As proposed previously, we believe this high neuronal density will translate to better neural recording although functional studies are required to understand the impact of L1 on chronic neural recording in the SC and DRG. As part of a combination of approaches, L1 continues to show promise for improving the interface between implanted devices and neural tissue.

Acknowledgments

The authors wish to thank Simon Watkins, Ph.D. and the Center for Biologic Imaging of the University of Pittsburgh for providing confocal training and assistance. We also wish to thank Noah Snyder and Cassandra Weaver for proof-reading the article. Funding for this work was provided in part by the Department of Defense TATRC grant WB1XWH-07-1-0716 and the National Institute of Health R01NS062019.

References

1. Rothschild RM. Neuroengineering tools/applications for bidirectional interfaces, brain-computer interfaces, and neuroprosthetic implants - a review of recent progress. Front Neuroeng. 2010; 3:112. [PubMed: 21060801]
2. Ryu SI, Shenoy KV. Human cortical prostheses: lost in translation? Neurosurg Focus. 2009; 27:E5. [PubMed: 19569893]
3. Song YK, Patterson WR, Bull CW, Borton DA, Li Y, Nurmikko AV, et al. A brain implantable microsystem with hybrid RF/IR telemetry for advanced neuroengineering applications. Conf Proc IEEE Eng Med Biol Soc. 2007; 2007:445–448. [PubMed: 18001985]
4. Morrell M. Brain stimulation for epilepsy: can scheduled or responsive neurostimulation stop seizures? Curr Opin Neurol. 2006; 19:164–168. [PubMed: 16538091]
5. Skarpaas TL, Morrell MJ. Intracranial stimulation therapy for epilepsy. Neurotherapeutics. 2009; 6:238–243. [PubMed: 19332315]
6. Pena C, Bowsher K, Costello A, De Luca R, Doll S, Li K, et al. An overview of FDA medical device regulation as it relates to deep brain stimulation devices. IEEE Trans Neural Syst Rehabil Eng. 2007; 15:421–424. [PubMed: 17894274]
7. Waltz JM. Spinal cord stimulation: a quarter century of development and investigation. A review of its development and effectiveness in 1,336 cases. Stereotact Funct Neurosurg. 1997; 69:288–299. [PubMed: 9711769]
8. Mushahwar VK, Gillard DM, Gauthier MJ, Prochazka A. Intraspinal micro stimulation generates locomotor-like and feedback-controlled movements. IEEE Trans Neural Syst Rehabil Eng. 2002; 10:68–81. [PubMed: 12173741]
9. Moritz CT, Lucas TH, Perlmutter SI, Fetz EE. Forelimb movements and muscle responses evoked by microstimulation of cervical spinal cord in sedated monkeys. J Neurophysiol. 2007; 97:110–120. [PubMed: 16971685]
10. Weber DJ, Stein RB, Everaert DG, Prochazka A. Limb-state feedback from ensembles of simultaneously recorded dorsal root ganglion neurons. J Neural Eng. 2007; 4:S168–S180. [PubMed: 17873416]
11. Gaunt RA, Hokanson JA, Weber DJ. Microstimulation of primary afferent neurons in the L7 dorsal root ganglia using multielectrode arrays in anesthetized cats: thresholds and recruitment properties. J Neural Eng. 2009; 6:055009. [PubMed: 19721181]
12. Schwartz AB. Cortical neural prosthetics. Annu Rev Neurosci. 2004; 27:487–507. [PubMed: 15217341]
13. Schwartz AB, Cui XT, Weber DJ, Moran DW. Brain-controlled interfaces: movement restoration with neural prosthetics. Neuron. 2006; 52:205–220. [PubMed: 17015237]
14. Cheung KC. Implantable microscale neural interfaces. Biomed Microdevices. 2007; 9:923–938. [PubMed: 17252207]
15. Polikov VS, Tresco PA, Reichert WM. Response of brain tissue to chronically implanted neural electrodes. J Neurosci Methods. 2005; 148:1–18. [PubMed: 16198003]

16. Rao SS, Winter JO. Adhesion molecule-modified biomaterials for neural tissue engineering. Front Neuroeng. 2009; 2:6. [PubMed: 19668707]
17. Straley KS, Heilshorn SC. Design and adsorption of modular engineered proteins to prepare customized, neuron-compatible coatings. Front Neuroeng. 2009; 2:9. [PubMed: 19562090]
18. Grill WM, Norman SE, Bellamkonda RV. Implanted neural interfaces: biochallenges and engineered solutions. Annu Rev Biomed Eng. 2009; 11:1–24. [PubMed: 19400710]
19. Azemi E, Stauffer WR, Gostock MS, Lagenaur CF, Cui XT. Surface immobilization of neural adhesion molecule L1 for improving the biocompatibility of chronic neural probes: In vitro characterization. Acta Biomater. 2008; 4:1208–1217. [PubMed: 18420473]
20. Panetsos F, Avendano C, Negredo P, Castro J, Bonacasa V. Neural prostheses: electrophysiological and histological evaluation of central nervous system alterations due to long-term implants of sieve electrodes to peripheral nerves in cats. IEEE Trans Neural Syst Rehabil Eng. 2008; 16:223–232. [PubMed: 18586601]
21. Pardue MT, Stubbs EB Jr, Perlman JI, Narfstrom K, Chow AY, Peachey NS. Immunohistochemical studies of the retina following long-term implantation with subretinal microphotodiode arrays. Exp Eye Res. 2001; 73:333–343. [PubMed: 11520108]
22. Lago N, Udina E, Ramachandran A, Navarro X. Neurobiological assessment of regenerative electrodes for bidirectional interfacing injured peripheral nerves. IEEE Trans Biomed Eng. 2007; 54:1129–1137. [PubMed: 17554832]
23. Azemi E, Lagenaur CF, Cui XT. The surface immobilization of the neural adhesion molecule L1 on neural probes and its effect on neuronal density and gliosis at the probe/tissue interface. Biomaterials. 2011; 32:681–692. [PubMed: 20933270]
24. Maness PF, Schachner M. Neural recognition molecules of the immunoglobulin superfamily: signaling transducers of axon guidance and neuronal migration. Nat Neurosci. 2007; 10:19–26. [PubMed: 17189949]
25. Figge C, Loers G, Schachner M, Tilling T. Neurite outgrowth triggered by the cell adhesion molecule L1 requires activation and inactivation of the cytoskeletal protein cofilin. Mol Cell Neurosci. 2011
26. Lemmon V, Farr KL, Lagenaur C. L1-mediated axon outgrowth occurs via a homophilic binding mechanism. Neuron. 1989; 2:1597–1603. [PubMed: 2627381]
27. Lagenaur C, Lemmon V. An L1-like molecule, the 8D9 antigen, is a potent substrate for neurite extension. Proc Natl Acad Sci U S A. 1987; 84:7753–7757. [PubMed: 3478724]
28. Kenwrick S, Watkins A, De Angelis E. Neural cell recognition molecule L1: relating biological complexity to human disease mutations. Hum Mol Genet. 2000; 9:879–886. [PubMed: 10767310]
29. Nishimune H, Bernreuther C, Carroll P, Chen S, Schachner M, Henderson CE. Neural adhesion molecules L1 and CHL1 are survival factors for motoneurons. J Neurosci Res. 2005; 80:593–599. [PubMed: 15880726]
30. Vutskits L, Djebbara-Hannas Z, Zhang H, Paccaud JP, Durbec P, Rougon G, et al. PSA-NCAM modulates BDNF-dependent survival and differentiation of cortical neurons. Eur J Neurosci. 2001; 13:1391–1402. [PubMed: 11298800]
31. Hulley P, Schachner M, Lubbert H. L1 neural cell adhesion molecule is a survival factor for fetal dopaminergic neurons. J Neurosci Res. 1998; 53:129–134. [PubMed: 9671969]
32. Aubert I, Ridet JL, Gage FH. Regeneration in the adult mammalian CNS: guided by development. Curr Opin Neurobiol. 1995; 5:625–635. [PubMed: 8580714]
33. Xu JC, Bernreuther C, Cui YF, Jakovcevski I, Hargus G, Xiao MF, et al. Transplanted L1 expressing radial glia and astrocytes enhance recovery after spinal cord injury. J Neurotrauma. 2011; 28:1921–1937. [PubMed: 21671795]
34. Cui YF, Xu JC, Hargus G, Jakovcevski I, Schachner M, Bernreuther C. Embryonic stem cell-derived L1 overexpressing neural aggregates enhance recovery after spinal cord injury in mice. PLoS One. 2011; 6:e17126. [PubMed: 21445247]
35. Lavdas AA, Chen J, Papastefanaki F, Chen S, Schachner M, Matsas R, et al. Schwann cells engineered to express the cell adhesion molecule L1 accelerate myelination and motor recovery after spinal cord injury. Exp Neurol. 2010; 221:206–216. [PubMed: 19909742]

36. Takeda Y, Murakami Y, Asou H, Uyemura K. The roles of cell adhesion molecules on the formation of peripheral myelin. Keio J Med. 2001; 50:240–248. [PubMed: 11806501]
37. Mackintosh JA, Veal DA, Karuso P. Fluoroprofile, a fluorescence-based assay for rapid and sensitive quantitation of proteins in solution. Proteomics. 2005; 5:4673–4677. [PubMed: 16267819]
38. Musallam S, Bak MJ, Troyk PR, Andersen RA. A floating metal microelectrode array for chronic implantation. J Neurosci Methods. 2007; 160:122–127. [PubMed: 17067683]
39. Brewer GJ. Serum-free B27/neurobasal medium supports differentiated growth of neurons from the striatum, substantia nigra, septum, cerebral cortex, cerebellum, and dentate gyrus. J Neurosci Res. 1995; 42:674–683. [PubMed: 8600300]
40. Cheepsunthorn P, Radov L, Menzies S, Reid J, Connor JR. Characterization of a novel brain-derived microglial cell line isolated from neonatal rat brain. Glia. 2001; 35:53–62. [PubMed: 11424192]
41. Luo X, Matranga C, Tan S, Alba N, Cui XT. Carbon nanotube nanoreservior for controlled release of anti-inflammatory dexamethasone. Biomaterials. 2011; 32:6316–6323. [PubMed: 21636128]
42. Ito D, Imai Y, Ohsawa K, Nakajima K, Fukuuchi Y, Kohsaka S. Microglia-specific localisation of a novel calcium binding protein, Iba1. Brain Res Mol Brain Res. 1998; 57:1–9. [PubMed: 9630473]
43. Patro N, Nagayach A, Patro IK. Iba1 expressing microglia in the dorsal root ganglia become activated following peripheral nerve injury in rats. Indian J Exp Biol. 2010; 48:110–116. [PubMed: 20455319]
44. Ohsawa K, Neo M, Matsuoka H, Akiyama H, Ito H, Kohno H, et al. The expression of bone matrix protein mRNAs around beta-TCP particles implanted into bone. J Biomed Mater Res. 2000; 52:460–466. [PubMed: 11007613]
45. Ito D, Tanaka K, Suzuki S, Dembo T, Fukuuchi Y. Enhanced expression of Iba1, ionized calcium-binding adapter molecule 1, after transient focal cerebral ischemia in rat brain. Stroke. 2001; 32:1208–1215. [PubMed: 11340235]
46. Mori I, Goshima F, Koshizuka T, Imai Y, Kohsaka S, Koide N, et al. Iba1-expressing microglia respond to herpes simplex virus infection in the mouse trigeminal ganglion. Brain Res Mol Brain Res. 2003; 120:52–56. [PubMed: 14667577]
47. Dumont RJ, Okonkwo DO, Verma S, Hurlbert RJ, Boulos PT, Ellegala DB, et al. Acute spinal cord injury, part I: pathophysiologic mechanisms. Clin Neuropharmacol. 2001; 24:254–264. [PubMed: 11586110]
48. Paterniti I, Genovese T, Crisafulli C, Mazzon E, Di Paola R, Galuppo M, et al. Treatment with green tea extract attenuates secondary inflammatory response in an experimental model of spinal cord trauma. Naunyn Schmiedebergs Arch Pharmacol. 2009; 380:179–192. [PubMed: 19337722]
49. Majno G, Joris I. Apoptosis, oncosis, and necrosis. An overview of cell death. Am J Pathol. 1995; 146:3–15. [PubMed: 7856735]
50. Nicotera P, Ankarcrona M, Bonfoco E, Orrenius S, Lipton SA. Neuronal necrosis and apoptosis: two distinct events induced by exposure to glutamate or oxidative stress. Adv Neurol. 1997; 72:95–101. [PubMed: 8993688]
51. Liu XZ, Xu XM, Hu R, Du C, Zhang SX, McDonald JW, et al. Neuronal and glial apoptosis after traumatic spinal cord injury. J Neurosci. 1997; 17:5395–5406. [PubMed: 9204923]
52. Beattie MS, Farooqui AA, Bresnahan JC. Review of current evidence for apoptosis after spinal cord injury. J Neurotrauma. 2000; 17:915–925. [PubMed: 11063057]
53. Amemiya S, Kamiya T, Nito C, Inaba T, Kato K, Ueda M, et al. Anti-apoptotic and neuroprotective effects of edaravone following transient focal ischemia in rats. Eur J Pharmacol. 2005; 516:125–130. [PubMed: 15921675]
54. Oyinbo CA. Secondary injury mechanisms in traumatic spinal cord injury: a nugget of this multiply cascade. Acta Neurobiol Exp (Wars). 2011; 71:281–299. [PubMed: 21731081]
55. Bennett DL, Michael GJ, Ramachandran N, Munson JB, Averill S, Yan Q, et al. A distinct subgroup of small DRG cells express GDNF receptor components and GDNF is protective for these neurons after nerve injury. J Neurosci. 1998; 18:3059–3072. [PubMed: 9526023]

56. Hu P, Bembrick AL, Keay KA, McLachlan EM. Immune cell involvement in dorsal root ganglia and spinal cord after chronic constriction or transection of the rat sciatic nerve. Brain Behav Immun. 2007; 21:599–616. [PubMed: 17187959]
57. Hanani M. Satellite glial cells in sensory ganglia: from form to function. Brain Res Brain Res Rev. 2005; 48:457–476. [PubMed: 15914252]
58. Keast JR, Stephensen TM. Glutamate and aspartate immunoreactivity in dorsal root ganglion cells supplying visceral and somatic targets and evidence for peripheral axonal transport. J Comp Neurol. 2000; 424:577–587. [PubMed: 10931482]
59. Turner JN, Shain W, Szarowski DH, Andersen M, Martins S, Isaacson M, et al. Cerebral astrocyte response to micromachined silicon implants. Exp Neurol. 1999; 156:33–49. [PubMed: 10192775]
60. Georges PC, Miller WJ, Meaney DF, Sawyer ES, Janmey PA. Matrices with compliance comparable to that of brain tissue select neuronal over glial growth in mixed cortical cultures. Biophys J. 2006; 90:3012–3018. [PubMed: 16461391]
61. Amsden B. Curable, biodegradable elastomers: emerging biomaterials for drug delivery and tissue engineering. Soft Matter. 2007; 3:1335–1348.
62. Tew, GNaNS-D.; Agrawal, SK.; Bhatia, SR. New properties from PLA-PEO-PLA hydrogels. Soft Matter. 2005; 1:253–258.
63. Ware T, Simon D, Arreaga-Salas DE, Reeder J, Rennaker R, Keefer EW, et al. Fabrication of Responsive, Softening Neural Interfaces. Advanced Functional Materials. 2012 n/a-n/a.
64. Capadona JR, Shanmuganathan K, Tyler DJ, Rowan SJ, Weder C. Stimuli-responsive polymer nanocomposites inspired by the sea cucumber dermis. Science. 2008; 319:1370–1374. [PubMed: 18323449]
65. Harris JP, Capadona JR, Miller RH, Healy BC, Shanmuganathan K, Rowan SJ, et al. Mechanically adaptive intracortical implants improve the proximity of neuronal cell bodies. J Neural Eng. 2011; 8:066011. [PubMed: 22049097]
66. Harris JP, Hess AE, Rowan SJ, Weder C, Zorman CA, Tyler DJ, et al. In vivo deployment of mechanically adaptive nanocomposites for intracortical microelectrodes. J Neural Eng. 2011; 8:046010. [PubMed: 21654037]
67. Irintchev A, Schachner M. The Injured and Regenerating Nervous System: Immunoglobulin Superfamily Members as Key Players. Neuroscientist. 2011
68. Becker CG, Lieberoth BC, Morellini F, Feldner J, Becker T, Schachner M. L1.1 is involved in spinal cord regeneration in adult zebrafish. J Neurosci. 2004; 24:7837–7842. [PubMed: 15356195]
69. Becker T, Lieberoth BC, Becker CG, Schachner M. Differences in the regenerative response of neuronal cell populations and indications for plasticity in intraspinal neurons after spinal cord transection in adult zebrafish. Mol Cell Neurosci. 2005; 30:265–278. [PubMed: 16098761]
70. Chen J, Bernreuther C, Dihne M, Schachner M. Cell adhesion molecule l1-transfected embryonic stem cells with enhanced survival support regrowth of corticospinal tract axons in mice after spinal cord injury. J Neurotrauma. 2005; 22:896–906. [PubMed: 16083356]
71. Cui YF, Hargus G, Xu JC, Schmid JS, Shen YQ, Glatzel M, et al. Embryonic stem cell-derived L1 overexpressing neural aggregates enhance recovery in Parkinsonian mice. Brain. 2010; 133:189–204. [PubMed: 19995872]
72. Barron KD. Microglia: history, cytology, and reactions. J Neurol Sci. 2003; 207:98. [PubMed: 12614938]
73. Schwartz M. Macrophages and microglia in central nervous system injury: are they helpful or harmful? J Cereb Blood Flow Metab. 2003; 23:385–394. [PubMed: 12679714]
74. Sofroniew MV, Vinters HV. Astrocytes: biology and pathology. Acta Neuropathol. 2010; 119:7–35. [PubMed: 20012068]
75. Szarowski DH, Andersen MD, Retterer S, Spence AJ, Isaacson M, Craighead HG, et al. Brain responses to micro-machined silicon devices. Brain Res. 2003; 983:23–35. [PubMed: 12914963]
76. Roonprapunt C, Huang W, Grill R, Friedlander D, Grumet M, Chen S, et al. Soluble cell adhesion molecule L1-Fc promotes locomotor recovery in rats after spinal cord injury. J Neurotrauma. 2003; 20:871–882. [PubMed: 14577865]

77. Webb K, Budko E, Neuberger TJ, Chen S, Schachner M, Tresco PA. Substrate-bound human recombinant L1 selectively promotes neuronal attachment and outgrowth in the presence of astrocytes and fibroblasts. Biomaterials. 2001; 22:1017–1028. [PubMed: 11352083]

78. He W, McConnell GC, Bellamkonda RV. Nanoscale laminin coating modulates cortical scarring response around implanted silicon microelectrode arrays. J Neural Eng. 2006; 3:316–326. [PubMed: 17124336]

79. Singh A, Ehteshami G, Massia S, He J, Storer RG, Raupp G. Glial cell and fibroblast cytotoxicity study on plasma-deposited diamond-like carbon coatings. Biomaterials. 2003; 24:5083–5089. [PubMed: 14568424]

80. Wadhwa R, Lagenaur CF, Cui XT. Electrochemically controlled release of dexamethasone from conducting polymer polypyrrole coated electrode. J Control Release. 2006; 110:531–541. [PubMed: 16360955]

81. Zhong Y, Bellamkonda RV. Controlled release of anti-inflammatory agent alpha-MSH from neural implants. J Control Release. 2005; 106:309–318. [PubMed: 15978692]

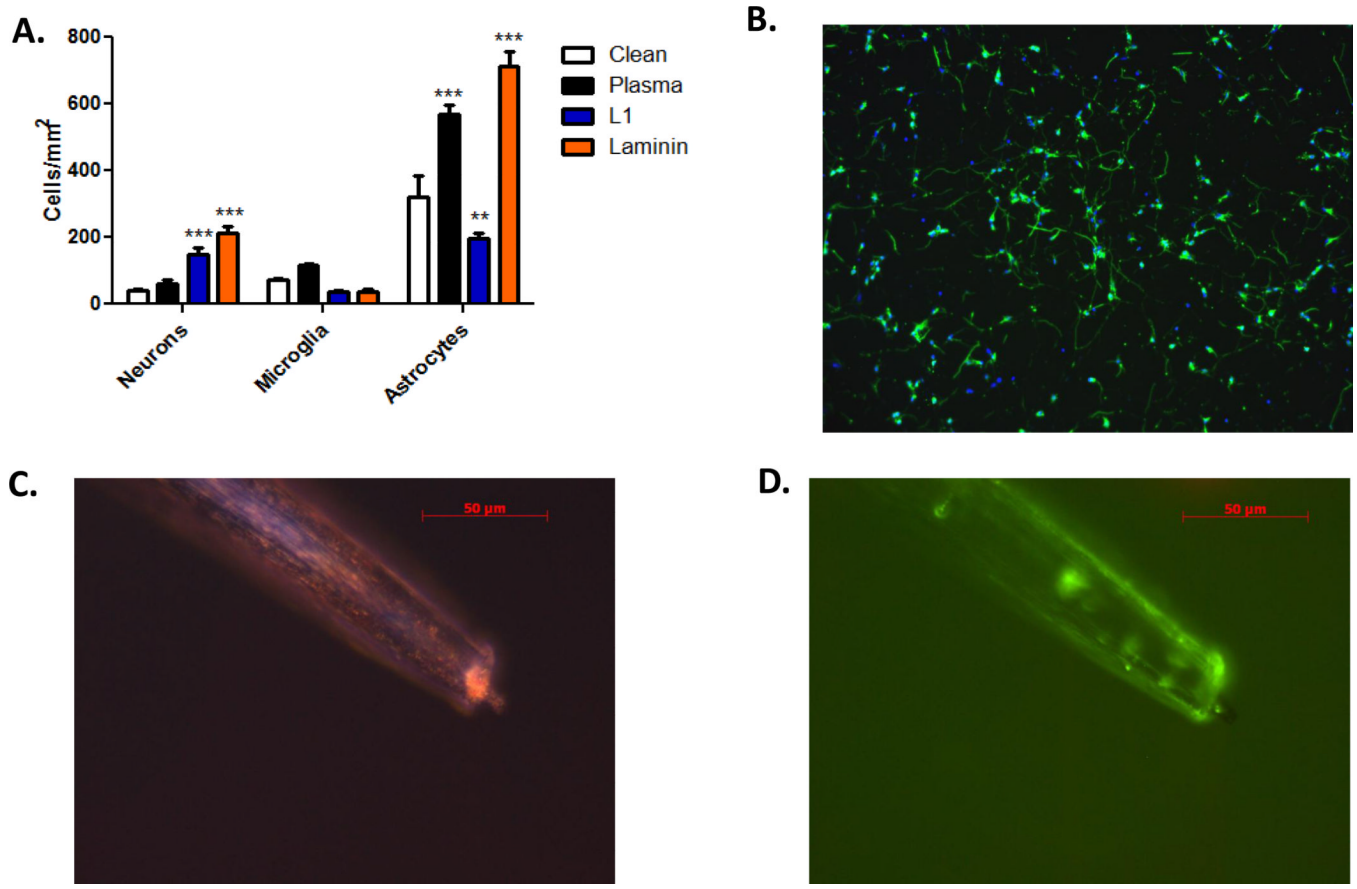

Figure 1.

Quantification of cell adhesion with different surface modifications. **A**: Parylene-C-treated microwires were added to primary neuron, microglia or astrocyte cultures and cell-type specific staining used to identify the cell types attached to each surface. Cell numbers were calculated by dividing the total number of cells by the surface area. Significant increases in neuronal adhesion were observed with L1 and laminin. Only the L1 coating showed a significant decrease in astrocyte adhesion. **B**: Representative images (10×) of neurons (green) and their nuclei (blue) on parylene-C coated samples treated with plasma + L1 after 5 days of soaking in media at physiological conditions. **C** and **D**: Representative images of plasma-treated microwires following antibody absorption. Bright-field (C) and fluorescence (D) microscopy images are provided with fluorescence images indicating localization of protein along the length of the electrode shaft. Error bars represent the mean ± standard error of the mean (SEM). $^{**}p < 0.01$; $^{***}p < 0.001$.

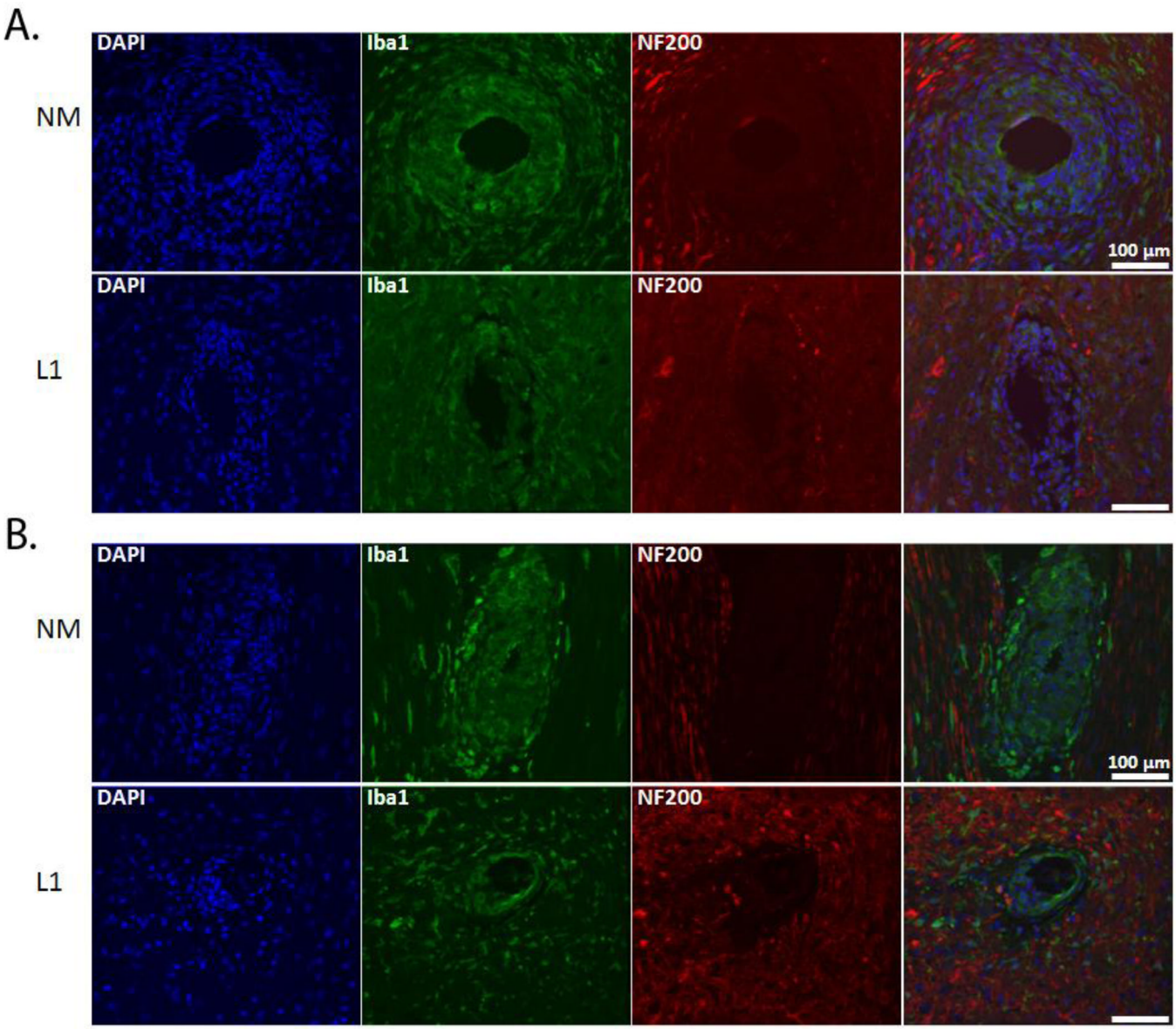

Figure 2.

NF-200 and Iba-1 expression in the spinal cord. Immunofluorescence images of rat SC stained for NF200 (red) and Iba1 (green) following implant of NM and L1-coated neural probes. NF200 staining was lacking in the area immediately surrounding the implant site and differences assessed by measuring the size of the area void of this staining. Iba1-positive cells were localized around the implant site and this increased immunoreactivity quantified and compared. **A**: Representative images at the 1 week (or acute) time point. **B**: Representative images at the 4 week (or chronic) time point. Scale bars represent 100 µm.

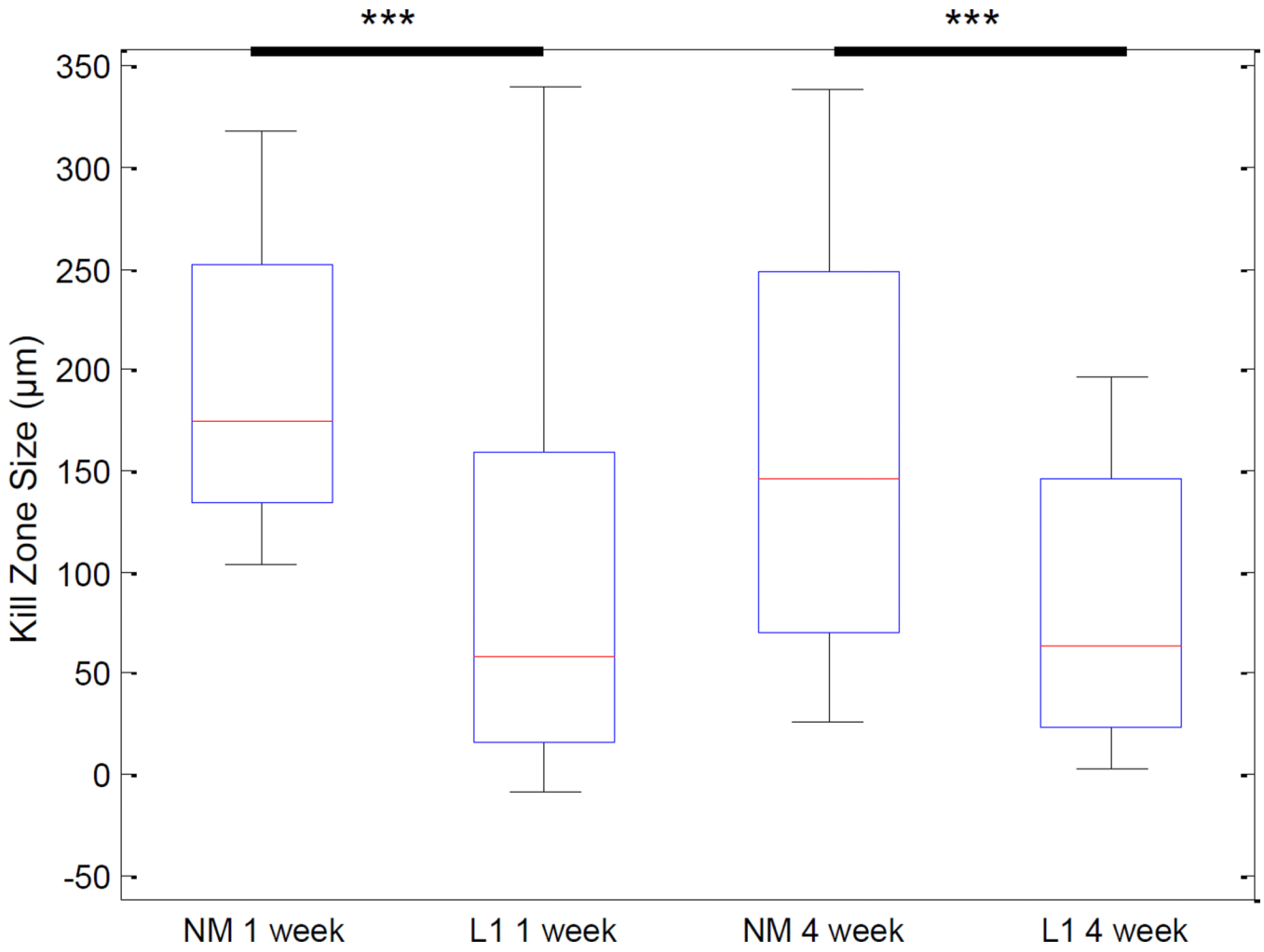

Figure 3.

Quantification of the kill zone size in the spinal cord. DAPI-stained images were used to define the perimeter of each implant and NF200-stained images used to identify the presence of neuronal processes. Kill zone size was computed in 10° bins around the 360° perimeter of the implant site by calculating the distance between the location of NF200 staining and the location of the implant. These distance measures were used to calculate the mean kill zone size and compared via the rank sum test. Significant decreases in kill zone size were observed with the L1 coating at both 1 week and 4 week time points. ***$p < 0.001$.

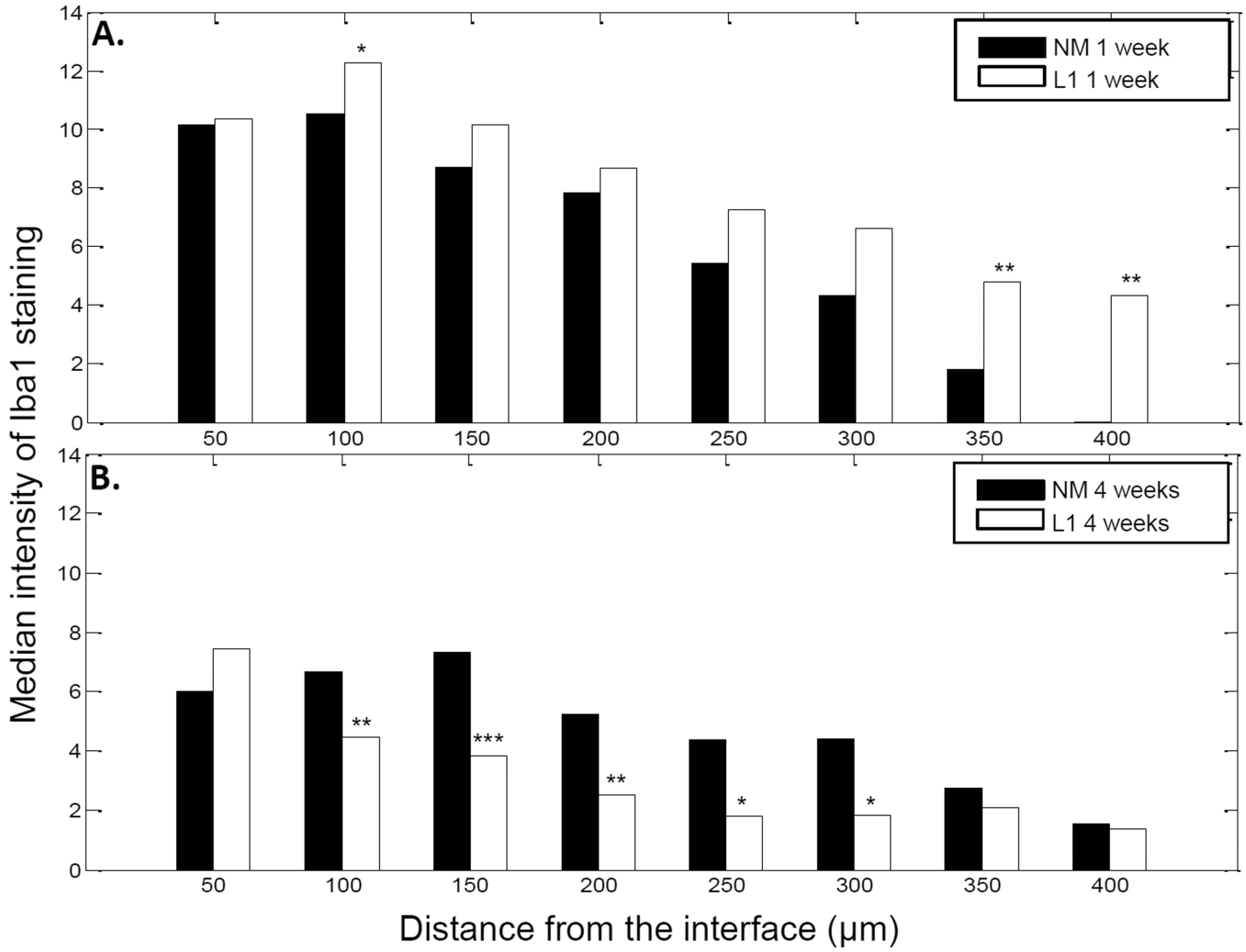

Figure 4.

Iba1 staining intensity as a function of distance from the electrode-tissue interface in the spinal cord. MATLAB was used to determine the decline in Iba1 staining intensity at 1 week (**A**) and 4 week (**B**) time points. The perimeter of the implant site was defined using the DAPI-stained images. Threshold values based on 95% of the background staining for each section were established, and Iba1 staining above this threshold measured as a function of distance from the implant site. The median intensity values were calculated in 50 μm bins and compared via the rank sum test. **A**: Significant increases were observed with the L1 coating at the 1 week time point. **B**: At 4 weeks, the L1 coating was associated with significant decreases in Iba1 staining. *$p < 0.05$; **$p < 0.01$; ***$p < 0.001$.

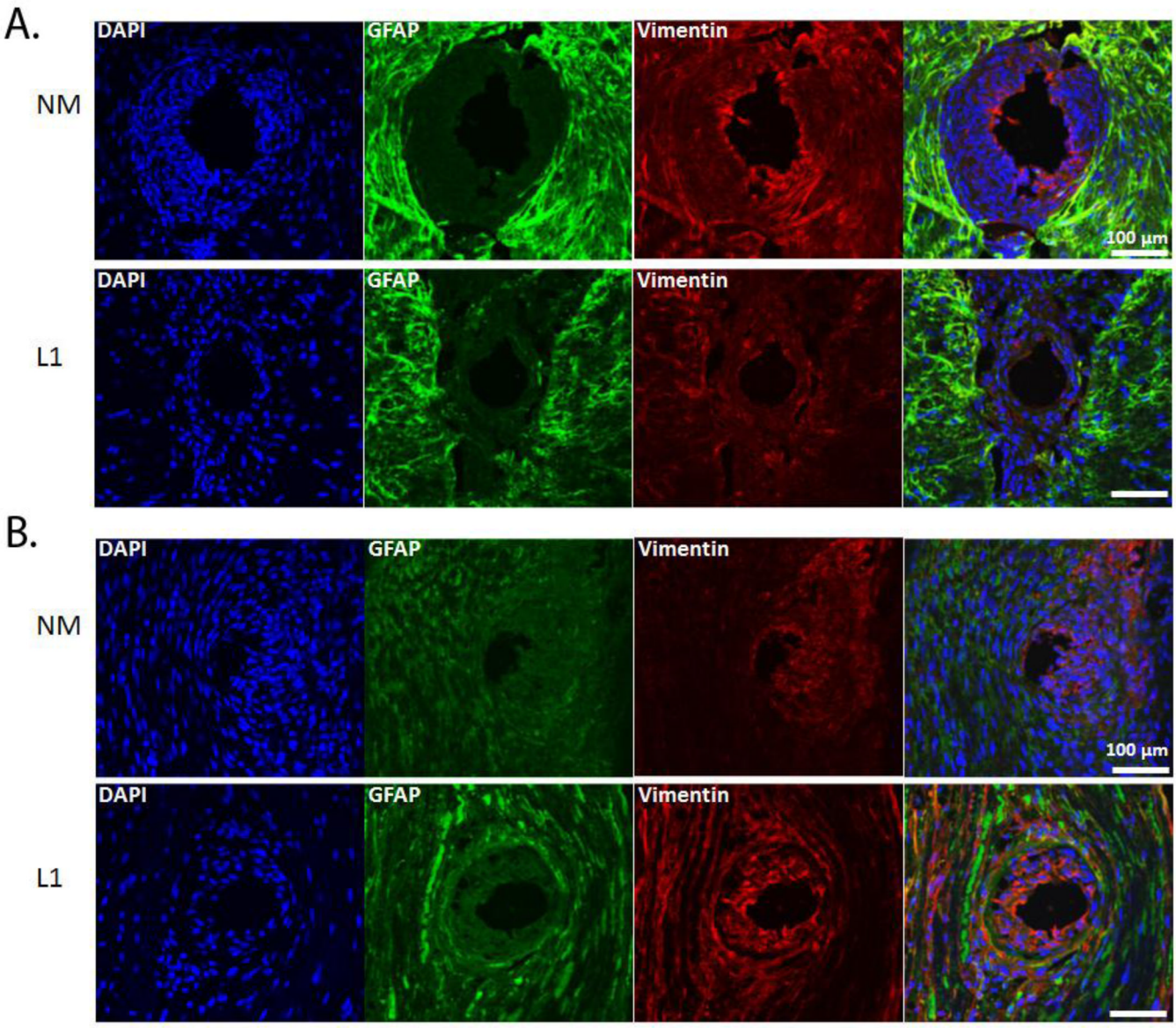

Figure 5.

GFAP and vimentin expression in spinal cord. Immunofluorescence images of rat SC stained for GFAP (green) and vimentin (red) following implant of NM and L1-coated neural probes. GFAP staining was characterized by the formation of a sheath not located to the area immediately surrounding the implant. Vimentin-positive cells were localized around the implant site with some co-localization with GFAP. **A**: Representative images at the 1 week (or acute) time point. **B**: Representative images at the 4 week (or chronic) time point. Scale bars represent 100 μm.

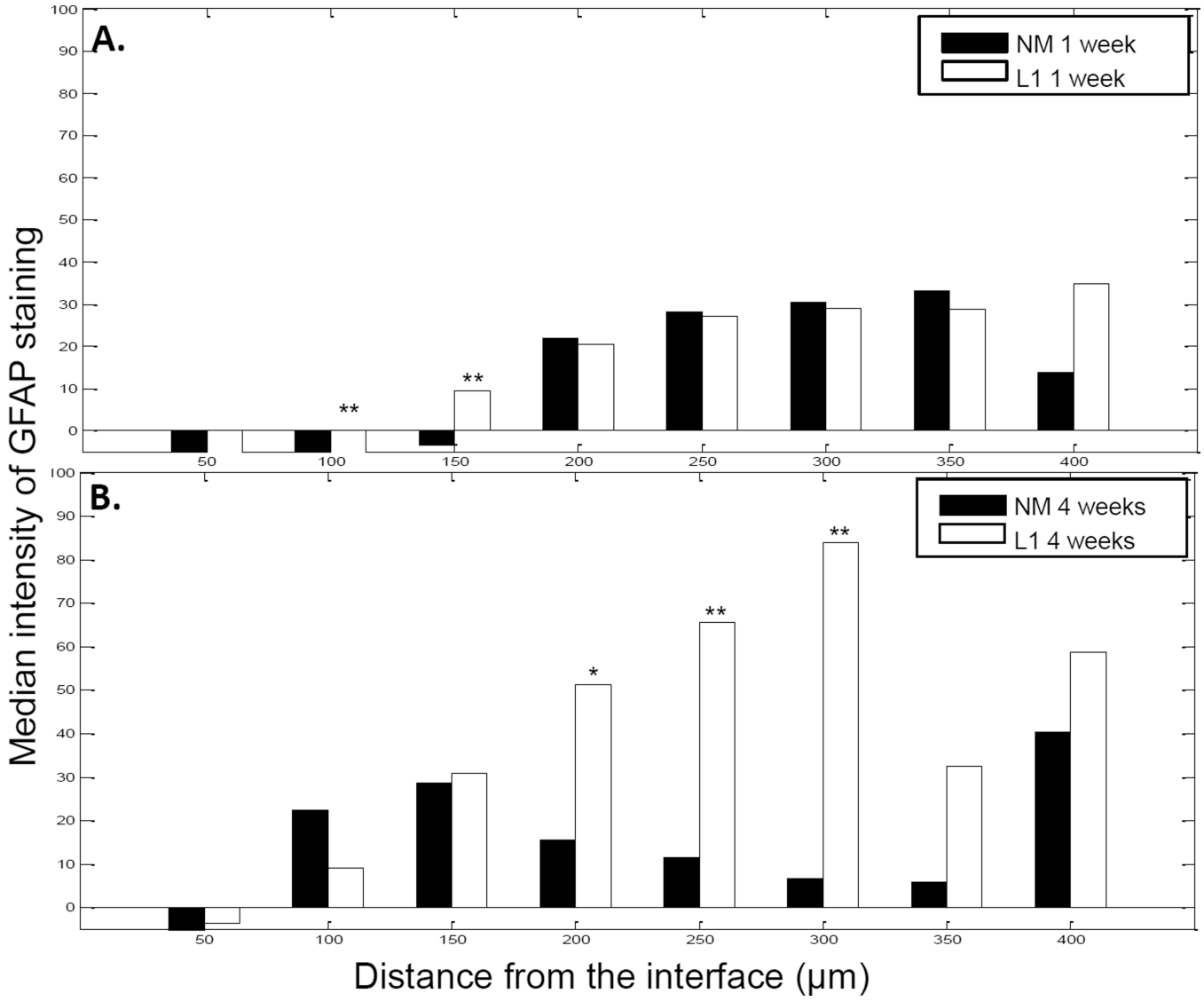

Figure 6.

GFAP staining intensity as a function of distance from the electrode-tissue interface in the spinal cord. MATLAB was used to determine the decline in GFAP staining intensity at 1 week (**A**) and 4 week (**B**) time points. The perimeter of the implant site was defined using the DAPI-stained images. Threshold values based on 95% of the background staining for each section were established and GFAP staining above this threshold measured as a function of distance from the implant site. The median intensity values were calculated in 50 μm bins and compared via the rank sum test. **A** and **B**: Significant increases were observed with the L1 coating at both 1 week and 4 weeks. *$p < 0.05$; **$p < 0.01$.

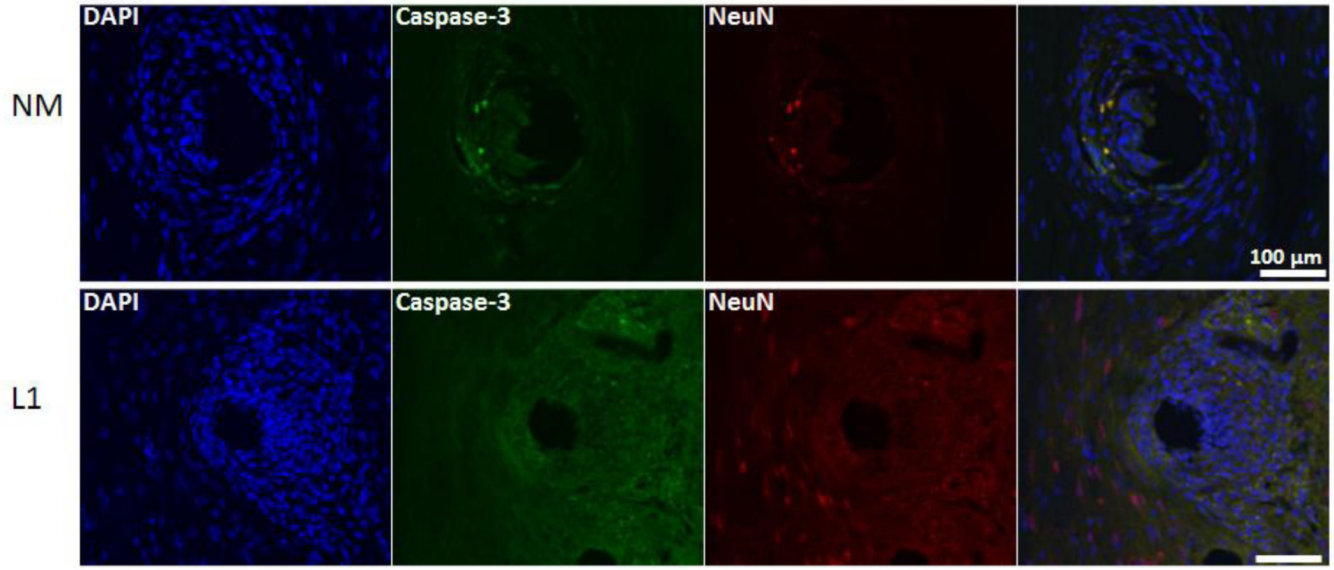

Figure 7.

Colocalization of NeuN and activated caspase-3 in the spinal cord. Immunofluorescence images were used to determine the degree of co-localization between NeuN (red) and cleaved caspase-3 (green) and representative images provided. The number of NeuN/caspase-3 positive cells was quantified and reported as a percentage of the total number of NeuN positive cells. Representative images are from the 1 week time point. Scale bars represent 100 μm.

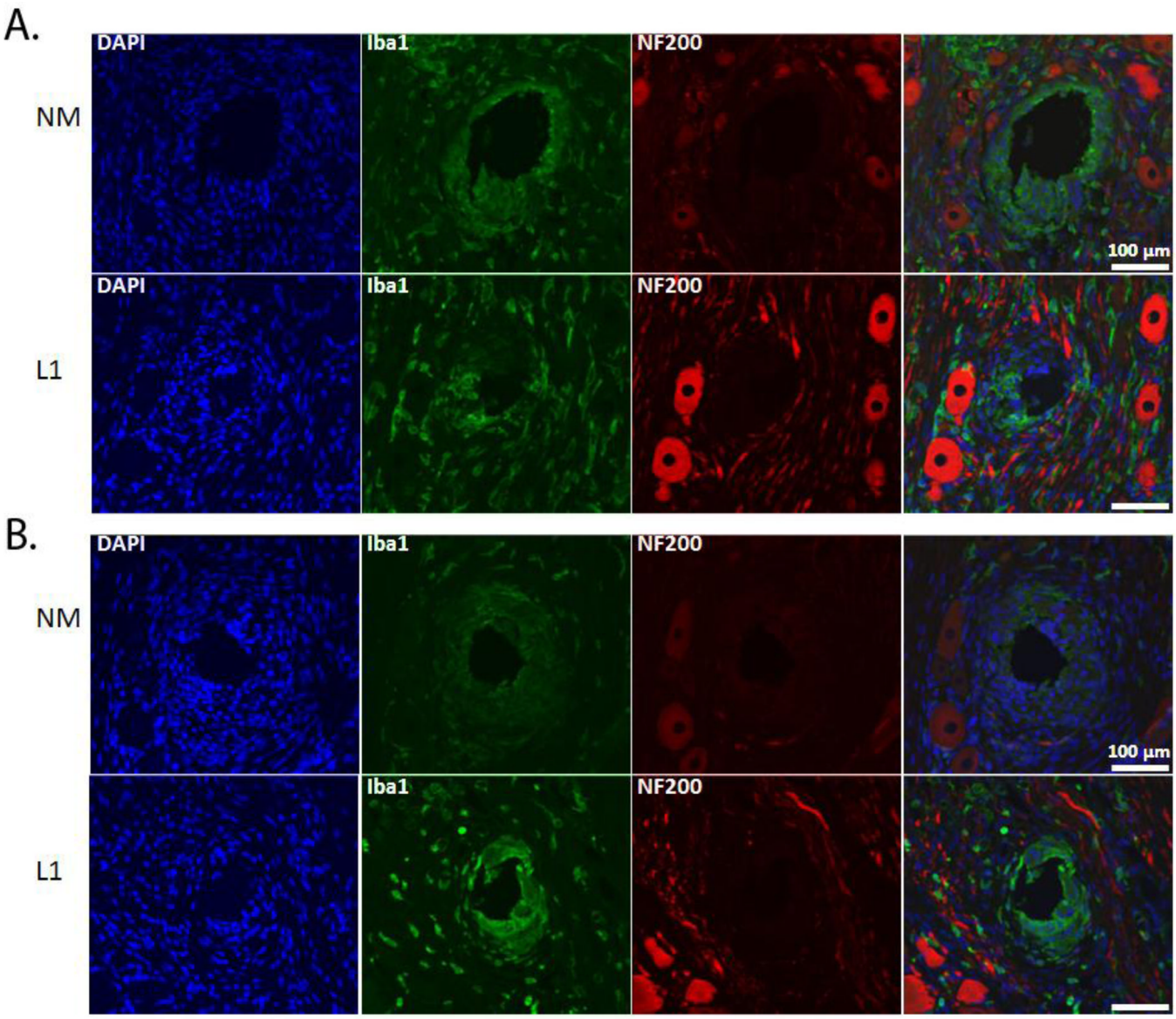

Figure 8.

NF-200 and Iba-1 expression in the dorsal root ganglion. Immunofluorescence images of rat DRG stained for NF200 (red) and Iba1 (green) following implant of NM and L1-coated neural probes. NF200 staining was lacking in the area immediately surrounding the implant site and differences assessed by measuring the size of the area void of this staining. Iba1-positive cells were localized around the implant site and this increased immunoreactivity quantified and compared. **A**: Representative images at the 1 week (or acute) time point. **B**: Representative images at the 4 week (or chronic) time point. Scale bars represent 100 μm.

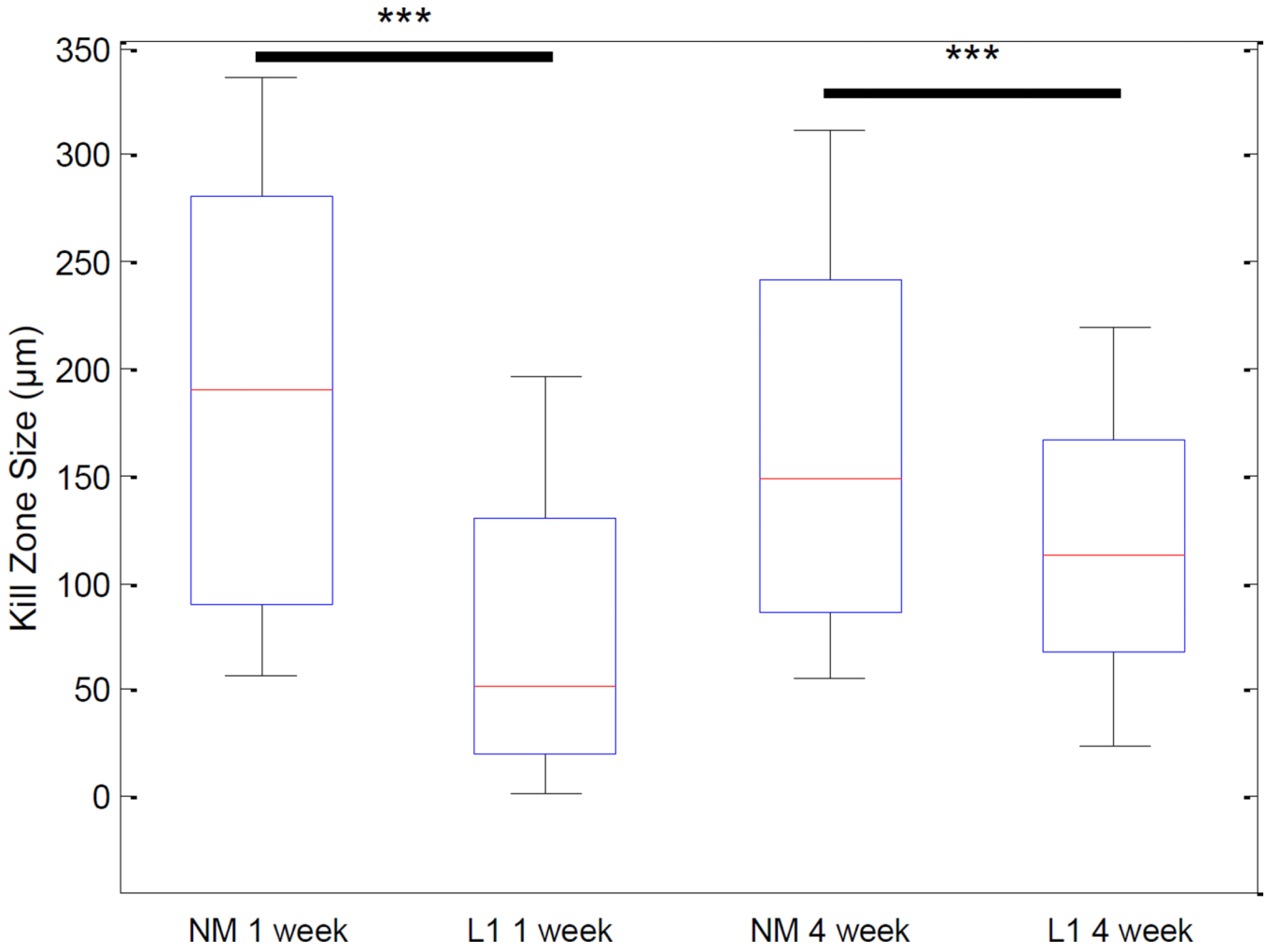

Figure 9.

Quantification of the kill zone size in the dorsal root ganglion. DAPI-stained images were used to define the perimeter of each implant and NF200-stained images used to identify the presence of neuronal processes. Kill zone size was computed in 10° bins around the 360° perimeter of the implant site by calculating the distance between the location of NF200 staining and the location of the implant. These distance measures were used to calculate the mean kill zone size and compared via the rank sum test. Significant decreases in kill zone size were observed with the L1 coating at both 1 week and 4 week time points. ***$p < 0.001$.

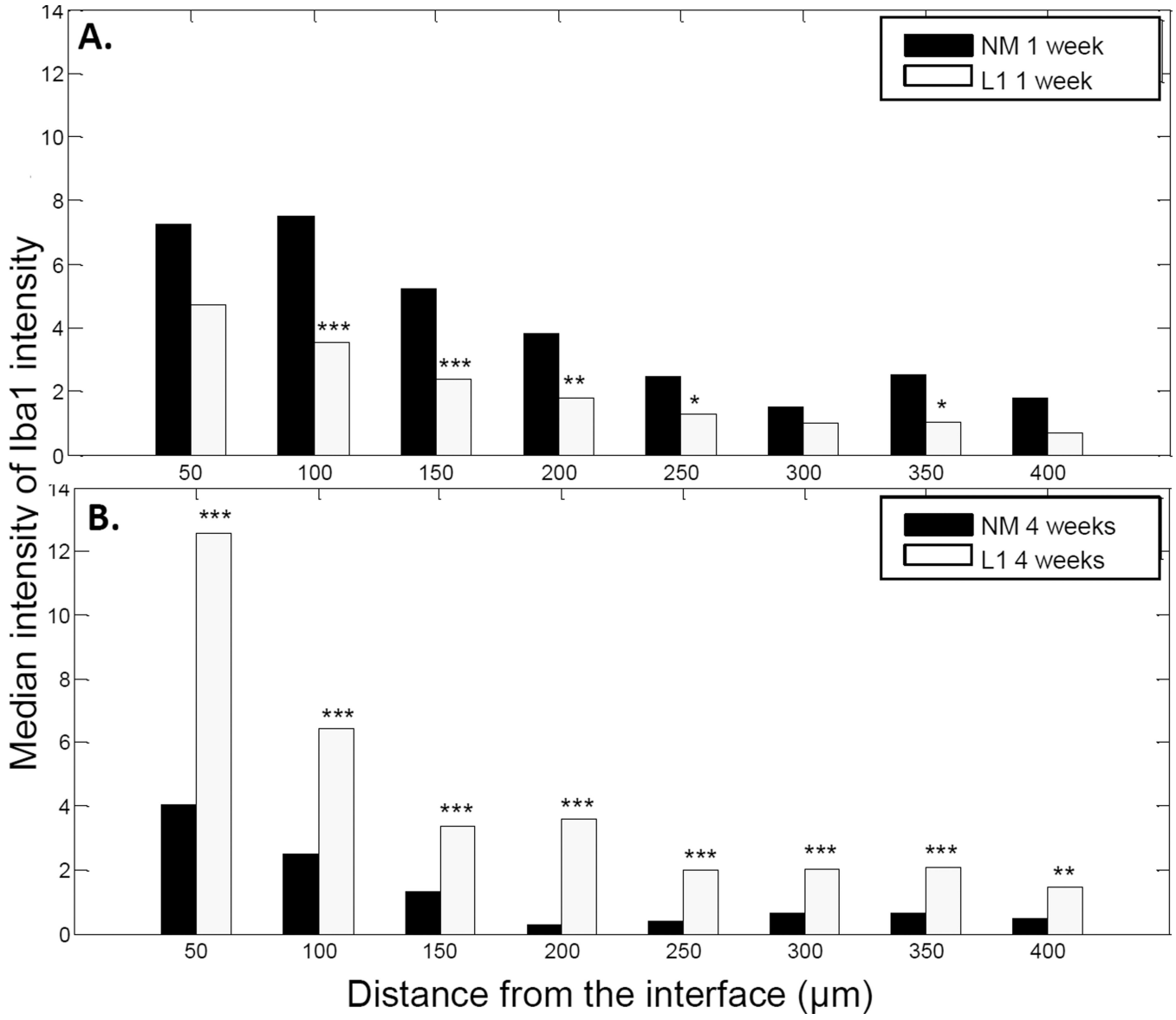

Figure 10.

Iba1 staining intensity as a function of distance from the electrode-tissue interface in the dorsal root ganglion. MATLAB was used to determine the decline in Iba1 staining intensity at 1 week (**A**) and 4 week (**B**) time points. The perimeter of the implant site was defined using the DAPI-stained images. Threshold values based on 95% of the background staining for each section were established, and Iba1 staining above this threshold measured as a function of distance from the implant site. The median intensity values were calculated in 50 μm bins and compared via the rank sum test. **A**: Significant decreases were observed with the L1 coating at the 1 week time point. **B**: At 4 weeks, the L1 coating was associated with significant increases in Iba1 staining. *$p < 0.05$; **$p < 0.01$; ***$p < 0.001$.

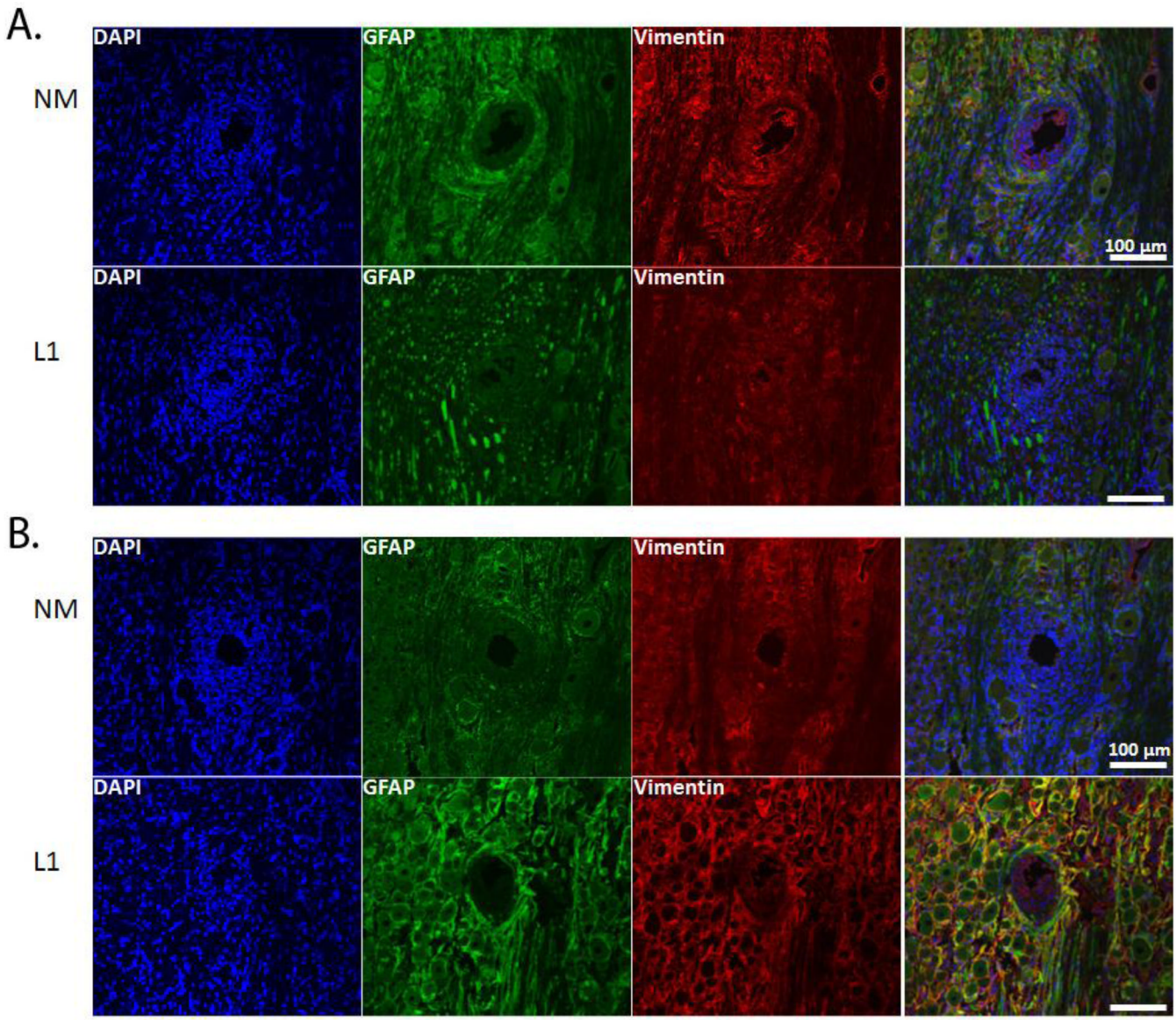

Figure 11.

GFAP and vimentin expression in the dorsal root ganglion. Immunofluorescence images of rat DRG stained for GFAP (green) and vimentin (red) following implant of NM and L1-coated neural probes. GFAP staining was characterized by the formation of a sheath not located to the area immediately surrounding the implant. Vimentin-positive cells were localized around the implant site with some co-localization with GFAP. **A**: Representative images at the 1 week (or acute) time point. **B**: Representative images at the 4 week (or chronic) time point. Scale bars represent 100 μm.

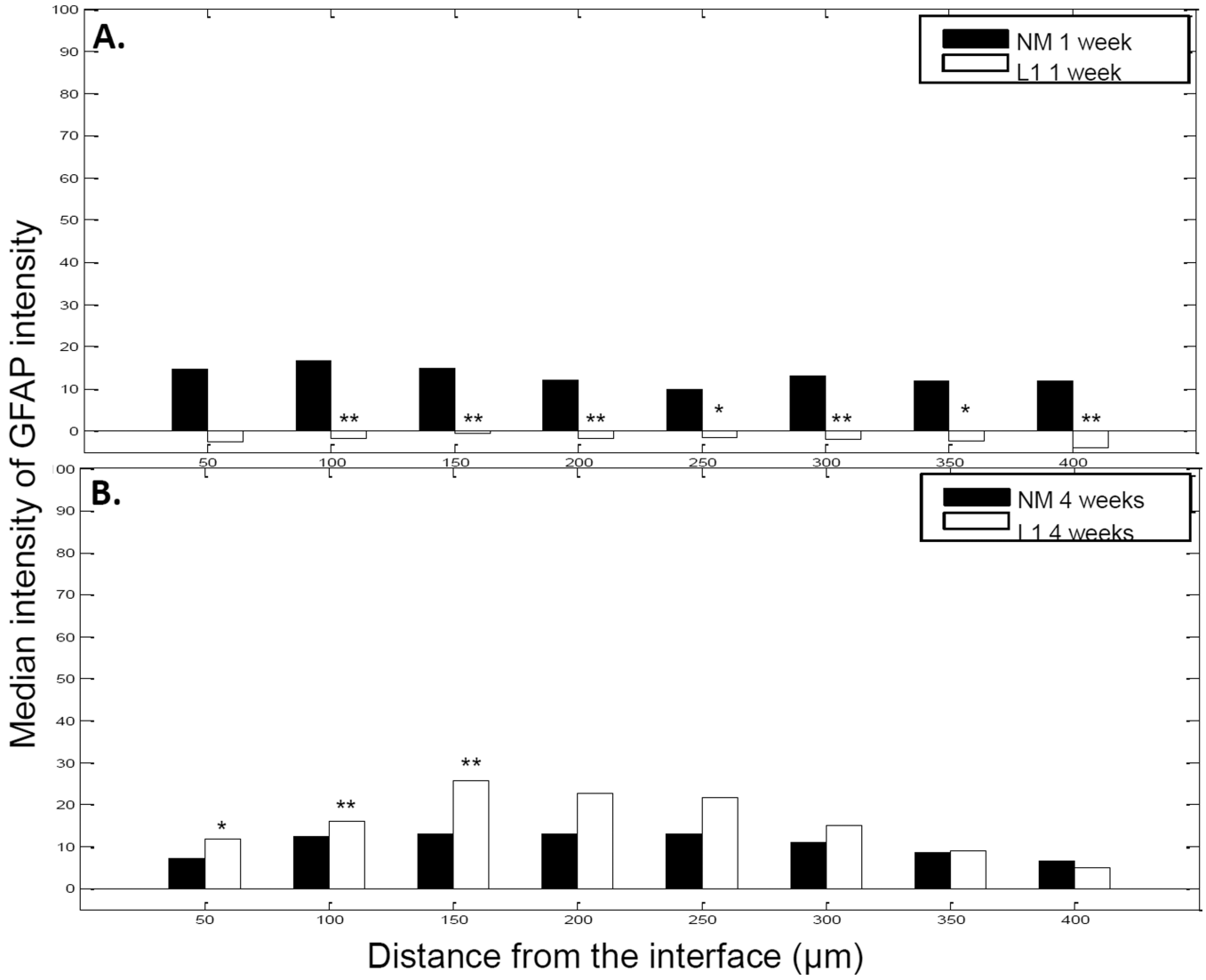

Figure 12.

GFAP staining intensity as a function of distance from the electrode-tissue interface in the dorsal root ganglion. MATLAB was used to determine the decline in GFAP staining intensity at 1 week (**A**) and 4 week (**B**) time points. The perimeter of the implant site was defined using the DAPI-stained images. Threshold values based on 95% of the background staining for each section were established and GFAP staining above this threshold measured as a function of distance from the implant site. The median intensity values were calculated in 50 μm bins and compared via the rank sum test. **A** and **B**: With L1, significant decreases were observed with the L1 coating at 1 week while significant increases were observed at 4 weeks. *$p < 0.05$; **$p < 0.01$.

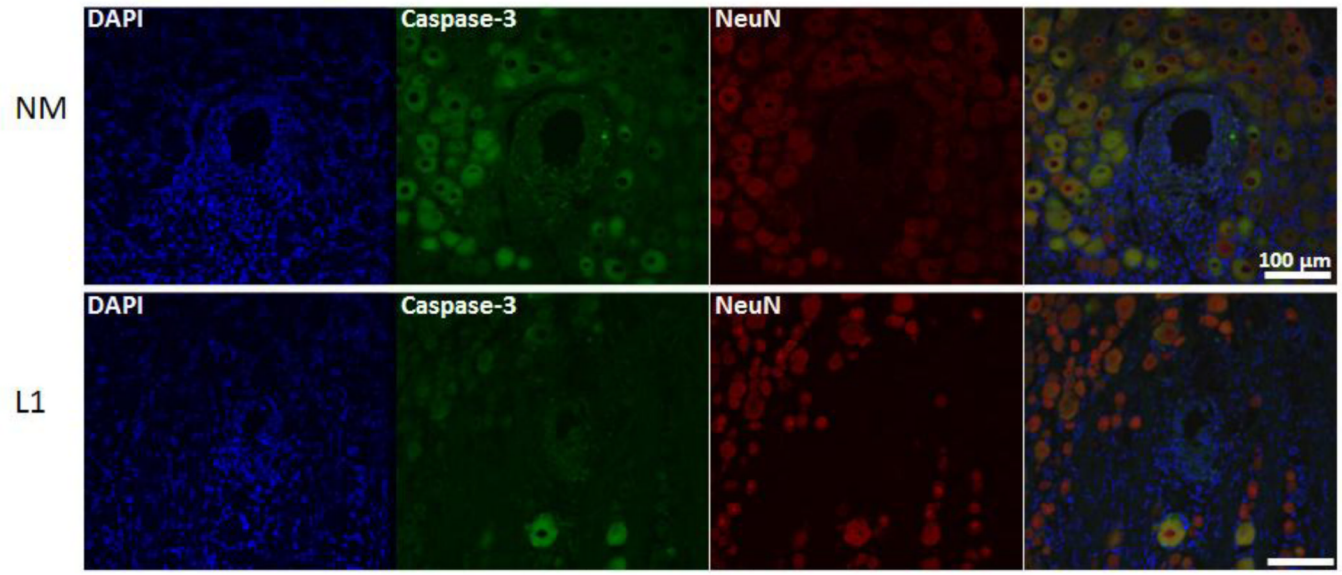

Figure 13.

Colocalization of NeuN and activated caspase-3 in the dorsal root ganglion. Immunofluorescence images were used to determine the degree of co-localization between NeuN (red) and cleaved caspase-3 (green) and representative images provided. The number of NeuN/caspase-3 positive cells was quantified and reported as a percentage of the total number of NeuN positive cells. Representative images are from the 1 week time point. Scale bars represent 100 μm.

Table 1

Animals in each treatment group

Site of Implant	Time Point	Number of Animals (NM)	Number of Electrodes	Number of Animals (L1)	Number of Electrodes
DRG	1 week	*n* = 3	*n* = 6	*n* = 3	*n* = 8
DRG	4 weeks	*n* = 3	*n* = 9	*n* = 3	*n* = 5
SC	1 week	*n* = 3	*n* = 7	*n* = 3	*n* = 7
SC	4 weeks	*n* = 4	*n* = 8	*n* = 3	*n* = 7

Table 2

Antibodies used for histological characterization

Antibody	Specificity
NF200	Mature axons
Iba1	Microglia/macrophages
GFAP	Astrocytes
Vimentin	Immature and reactive astrocytes, microglia, endothelial cells, fibroblasts
NeuN	Neuronal nuclei
Caspase-3	Cleaved (activated) caspase-3

Table 3

NeuN/Caspase-3 colocalization

Location	Time Point (week)	Coating Condition	Percentage of NeuN/Caspase-3 Positive Cells
SC	1	NM	11.3% (18 of 160)
		L1	5.1% (12 of 235)
	4	NM	21.8% (36 of 165)
		L1	7.0% (31 of 440)
DRG	1	NM	67.9% (142 of 209)
		L1	31.5% (23 of 73)
	4	NM	68.9% (51 of 74)
		L1	12.4% (31 of 249)